NASA Technical Memorandum 78589

Wind-Tunnel Investigation of a Large-Scale VTOL Aircraft Model With Wing Root and Wing Thrust Augmentors

Kiyoshi Aoyagi and Thomas N. Aiken

September 1979

National Aeronautics and Space Administration

NASA Technical Memorandum 78589

Wind-Tunnel Investigation of a Large-Scale VTOL Aircraft Model With Wing Root and Wing Thrust Augmentors

Kiyoshi Aoyagi
Thomas N. Aiken, Ames Research Center, Moffett Field, California

National Aeronautics and
Space Administration

Ames Research Center
Moffett Field, California 94035

SYMBOLS

b	wing span, m (ft)
C_D	drag coefficient, $\frac{\text{drag}}{q_\infty S}$
C_d	discharge area coefficient of augmentor nozzle
$(C_J)_{aug}$	augmentor gross thrust coefficient, $\frac{\phi_F \text{ (measured nozzle thrust)}_F + \phi_W \text{ (calculated nozzle thrust)}_W}{q_\infty S}$
$(C_J)_{nozzle}$	augmentor nozzle thrust coefficient $\left(\frac{\text{measured thrust}}{q_\infty S}\right)_F$, or $\left(\frac{\text{calculated thrust}}{q_\infty S}\right)_W$
C_L	lift coefficient, $\frac{\text{lift}}{q_\infty S}$
C_m	pitching-moment coefficient, $\frac{\text{pitching moment}}{q_\infty S\bar{c}}$
C_N	yawing-moment coefficient about stability axis, $\frac{\text{awing moment}}{q_\infty Sb}$
C_R	rolling-moment coefficient about stability axis, $\frac{\text{rolling moment}}{q_\infty Sb}$
C_Y	side-force coefficient about stability axis, $\frac{\text{side force}}{q_\infty S}$
c	wing chord measured parallel to the plane of symmetry, m (ft)
$\bar{c}$	mean aerodynamic chord of wing, $\frac{2}{S}\int_0^{b/2} c^2 dy$, m (ft)
DAR	augmentor diffuser ratio, $\frac{\text{augmentor exit area}}{\text{augmentor throat area}}$
i_t	horizontal tail incidence, deg
MAC	mean aerodynamic chord, m (ft)
P_F	duct static pressure for fuselage augmentor (see fig. 2(f)), N/m^2 (lb/ft^2)
P_N	duct static pressure for residual thrust orifice, N/m^2 (lb/ft^2)

P_0	absolute pressure of standard air, 101,315 N/m^2 (2116 lb/ft^2)
P_W	duct static pressure for wing augmentor, N/m^2 (lb/ft^2)
P_∞	free-stream static pressure, N/m^2 (lb/ft^2)
q_∞	free-stream dynamic pressure, N/m^2 (lb/ft^2)
RPR	$\frac{P_F}{P_\infty}$
S	wing area, m^2 (ft^2)
$(T)_{isentropic}$	wing root augmentor gross thrust based on rake pressure and temperature measurements (see fig. 6) assuming isentropic expansion to ambient pressure, N (lb)
WCP	wing chord plane
y	spanwise distance perpendicular to the plane of symmetry, m (ft)
α	angle of attack of fuselage, deg
β	angle of sideslip, deg
δ	absolute static-pressure ratio, $\frac{P}{P_o}$
δ_f	wing augmentor flap deflection, deg
η	wing semispan station, $\frac{y}{(b/2)}$
$'IN$	nozzle velocity coefficient, $\frac{\text{nozzle velocity obtained from mass flow and thrust measurements}}{\text{nozzle velocity obtained from isentropic expansion to ambient pressure}}$
ϕ_F	gross static thrust-augmentation ratio of wing root augmentor, $\frac{\text{measured augmentor thrust}}{\text{calculated nozzle thrust}}$
ϕ_W	gross static thrust-augmentation ratio of wing augmentor, $\frac{\text{measured augmentor thrust}}{\text{measured nozzle thrust}}$
$(\ )_F$	wing root augmentor
$(\ )_{RN}$	residual thrust of rear nozzle

$( )_W$	**wing** augmentor
$( )_U$	**uncorrected**

WIND-TUNNEL INVESTIGATION OF A LARGE-SCALE VTOL AIRCRAFT MODEL WITH WING ROOT AND WING THRUST AUGMENTORS

Kiyoshi Aoyagi and Thomas N. Aiken

Ames Research Center

SUMMARY

Tests were conducted in the Ames 40- by 80-Foot Wind Tunnel to determine the aerodynamic characteristics of a large-scale V/STOL aircraft model with thrust augmentors. The model had a double-delta wing of aspect ratio *(W)* 1.55 with augmentors located in the wing root and the wing trailing edge. The supply air for the augmentor primary nozzles was provided by the YJ-97 turbojet engine. The air flow was apportioned approximately 75% to the wing root augmentor and 24% to wing augmentor. Results were obtained at several trailing-edge flap deflections with the nozzle jet-momentum coefficients ranging from 0 to 7.9.

Three-component longitudinal data are presented with the augmentor operating with and without the horizontal tail. A limited amount of six-component data are also presented.

INTRODUCTION

Thrust augmentors are being considered in some V/STOL fighter aircraft designs (ref. 1). Reference 2 has shown several approaches of augmentor integration to this type of aircraft design. One arrangement, which is the subject of this investigation, is the combined use of wing root and wing flap augmentors with a double-delta wing planform. In this arrangement, the engine flow is diverted during hover to the augmentor nozzles at the wing root and also at the wing flap which is deflected at 90°. During the transition to forward flight, the flow to the wing root nozzles is gradually diverted to a tailpipe for thrust, while the wing flap is deflected back to provide circulatory lift, thrust, and pitch trim.

To investigate the augmentor flow-field effect on the aerodynamics during transition, a model was built which was powered by a YJ-97 engine. The engine had a flow split of 74% and 24% to the wing root and wing flap augmentors, respectively. A wind-tunnel investigation of this model was conducted in the Ames 40- by 80-Foot Wind Tunnel from hover to forward speed. Several wing augmentor deflections were tested with the wing root augmentor operating. Most of the data were obtained with the reference duct static-pressure ratio of 2.3 at dynamic pressures from 234.6 to 1857.7 N/m^2 (4.9 to 38.8 psf), with and without the horizontal tail. An analysis of the data is presented in reference 3.

This research program was undertaken in cooperation with the Canadian Department of National Defence and the de Havilland Aircraft of Canada.

MODEL AND APPARATUS

Photographs of the model in the Ames 40- by 80-Foot Wind Tunnel are shown in figures 1(a) through (d). Figures 1(a) and 1(b) show the model with the fuselage augmentor inlet and diffuser covered. Figure 1(c) shows the model with the fuselage augmentor nozzles, and figure 1(d) shows the model with the fuselage augmentor diffuser door deployed with the outboard door removed. Geometric details and pertinent dimensions of the model are shown in figure 2(a).

Fuselage

The fuselage had a length-to-maximum diameter ratio of 9.7. The nose section contained a 0.51 m (1.67 ft) internal diameter inlet for the YJ-97 turbojet engine with a large radius inlet lip. Exhaust gas ducting connected to the engine ran the full length of the fuselage. The exhaust gas was bled off from the exhaust duct to the wing root and wing augmentors, and the remainder was ducted to the trimming nozzle located at the aft end of the fuselage. The engine flow at PR = 3.0 was apportioned approximately as follows:

Wing root augmentor	74%
Wing augmentor	24%
Rear trimming nozzle	2%

Wing

The wing had a double-delta planform, a thickness-to-chord ratio of 6%, and AR of 1.65.

A wing augmentor flap was located at the wing trailing edge extending in the spanwise direction from 0.24 of the wing semispan to the wing tip. Details are discussed under wing augmentor.

Wing Root Augmentor

The geometry of the wing root augmentor and nozzles is given in table 1. The augmentor had a chordwise length of 2.49 m (8.16 ft) which was parallel to the model plane of symmetry, and a throat width of 0.27 m (0.875 ft). The center of the augmentor throat was located at 0.18 of the wing semispan. The diffuser normal exit width was 0.43 m (1.40 ft) and could be reduced to 0.27 m (0.875 ft) by moving the outboard diffuser door as shown in figure 2(b). The resulting diffuser area ratio was 1.60 and 1.00, respectively. No provision was made to vector the augmentor thrust with respect to the model;

The nozzles for the wing root augmentor had an AR (span-to-width) of 60 and an augmentor throat-to-nozzle area ratio of 22.5. They were designed to give an essentially vertical jet efflux. These nozzles were connected to

offtakes perpendicular to the exhaust gas ducting running down the center of the fuselage as shown in figure 2(c). To counteract the spanwise momentum of the flow in the nozzle, the exit plane was swept from 17° at the inboard end to 0° at the outboard end as shown in figure 2(d). The location of the nozzles in the augmentor was arranged to provide some BLC effect on the diffuser walls and on the augmentor end walls.

Wing Augmentor

The wing augmentor consisted of shrouds which extended from 0.24 to wing tip, and three geometrically different spanwise nozzle arrays as shown in figure 2(e). The geometry of the wing augmentor is shown in table 2. Since the shrouds tapered linearly with wing semispan, the augmentor throat size was optimized approximately at the midspan of each nozzle array. The wing augmentor could be deflected from 0° to 90° with the hinge line located at the supply-air-duct centerline.

The nozzles had an AR of 40 and a spacing-to-mean nozzle-width ratio of 8. These nozzles were connected to the tapered air-supply duct inside the wing and were oriented in the streamwise direction as shown in figure 2(e).

Air Supply

A GE YJ-97 turbojet engine supplied the high-pressure air for both the wing root and wing augmentor nozzles. An exhaust pressure (RPR) ratio ranging from 1.2 to 3.0 could be supplied by the engine. At an RPR of 3.0, the engine produced a thrust of about 20,017 N (4500 lb) with an effective nozzle area of about 0.071 m^2 (0.764 ft^2).

Tail

The geometry of the horizontal and vertical tails is given in figure 2(a). The all-movable horizontal tail was mounted on top of the vertical tail. The tail pivoted about its 0.27 MAC. Tail incidence could be varied from 5° to 15°.

CORRECTIONS

The data were corrected for wind-tunnel wall constraints. These corrections were determined by considering only the aerodynamic lift of the model ($C_{L_{AERO}}$) that resulted after the primary jet reaction components had been subtracted from the data as follows:

$$C_{L_{AERO}} = C_L - (C_J)_F \cos \alpha_u - (C_J)_W \sin (\alpha_U + \delta_f)$$

$$\alpha \simeq \alpha_u + 0.3538\ C_{L_{AERO}}$$

$$C_D = C_{D_u} + 0.0062\ C_{L_{AERO}}^2$$

$$C_m = C_{m_u} + 0.020\ C_{L_{AERO}} \text{ (horizontal tail on test only)}$$

The thrust values to compute C_J values with RPR were obtained from wind-tunnel scale measurements with the wing root augmentor, and from calculations with the wing augmentor. Duct pressures were obtained from the duct static-pressure tap shown in figure 2(f). Several rear nozzle orifice diameters were used to trim the engine during the investigation when the number of wing root-augmentor nozzles was reduced.

The data that are presented in this report are not corrected for engine ram drag.

TEST AND PROCEDURE

Static Augmentor Nozzle and Augmentor Thrust

The wing root-augmentor nozzle thrust calibration was determined statically from wind-tunnel scale measurements without the outboard diffuser door and with $\delta_f = 0"$ (see fig. 1(d)). Since the inlet fairings and fuselage side wall were on during the calibration, the thrust contribution due to the presence of these components was subtracted to obtain the nozzle thrust. This amounted to approximately 10%of the measured values as determined from a separate full-scale, cold-flow nozzle test. The nozzle static thrust of the wing augmentor was calculated on the basis of geometric nozzle area, wing duct stagnation pressure, and an estimated value of $\eta_N \cdot C_d$ which varied from 0.91 at PR = 1.5 to 0.93 at PR = 2.5.

The wing root-augmentor gross thrust was determined with the outboard diffuser door on and with $\delta_f = 0°$. Calibrations were obtained with none of the nozzles blanked off at a DAR of 1.6 and 1.0, and with a total of 14 and 26 nozzles blanked off separately at a DAR = 1.0. In the case where the nozzles were blanked off, every other nozzle was closed off starting with the second from the forward end.

The wing augmentor gross thrust was determined by subtracting the scale lift measurements obtained at $\delta_f = 0"$ and 90" with the wing augmentor operating.

Tests With Constant C_J and Varying Angle of Attack

A constant C_J value was maintained with an RPR of 2.3 in mostcasesas the angle of attack was varied for each wing augmentor flap deflection investigated. Flap deflections of 0°, 30°, and 90" were investigated with the wing root augmentor DAR of 1.6 and 1.0. The nominal C_J values were as follows:

AT PRIMARY NOZZLE

$(C_J)_{nozzle}$		q_∞	
Wing root	Wing	N/m^2	lb/ft^2
6.20	1.66	143.6	3.0
3.48	.92	234.6	4.9
1.74	.46	469.2	9.8
1.16	.31	708.6	14.8
.70	.19	1163.5	24.3
.44	.12	1857.7	38.8
0	0	703.8	14.7

During the investigation, parts of the wing root-augmentor primary nozzles at a DAR of 1.0 were blanked off to reduce the secondary flow and thus decrease the momentum drag. In one case, 7 nozzles out of 27 total in each fuselage augmentor were blanked off alternately starting with the second nozzle from the front. In the other case 13 nozzles were blanked off alternately starting with the second from the front and continuing to the rear. These nozzle arrangements will be referred to as 3/4- and 1/2-thrust output, respectively. A wing augmentor flap deflection of 60° was tested with the 3/4-thrust output, and flap deflection of 0°, 30°, and 60° were tested with the 1/2-thrust output. Tests were conducted with the wing-root-augmentor inlets covered and augmentor diffuser doors closed, and with the engine inoperative at flap deflection of 0" and 30°.

Tests With Varying C_J at Zero Angle of Attack

Values of C_J were varied by changing reference duct static-pressure ratios from 1.3 to 3.0 at a dynamic pressure ranging from 229.8 N/m^2 (4.8 lb/ft^2) to 1168.3 N/m^2 (24.4 lb/ft^2). Wing augmentor flap deflections of 0°, 30°, 60°, and 90" were tested with the wing root augmentor DAR of 1.6, and a deflection of 30° was tested with a DAR of 1.0. Flap deflections of 0° and 30" were tested at 1/2-thrust output.

Tests With Constant C_J and Varying Angle of Sideslip

A constant C_J was maintained at $\alpha_u = 0°$ at PR of 1.5 and 3.0, while β was varied from -12° to 12° for most cases. Tests were conducted with DAR of 1.6 and 1.0. Power-off data were obtained with the wing root augmentor inlet covered and the augmentor diffuser doors closed at a flap deflection of 30°.

RESULTS

The variations of augmentor-nozzle thrust with reference duct static-pressure ratio for the wing root and the wing augmentor at zero forward speed are shown in figures 3 and 4, respectively. The fuselage augmentor primary

thrusts were obtained from scale measurements, and the wing augmentor values were calculated by assuming an isentropic expansion to ambient pressure. The variation of the measured wing root augmentor gross-augmentation ratio with the reference duct static-pressure ratio at a DAR of 1.6 and 1.0 is shown in figure 5. The variations of the wing root augmentor ideal thrust with tunnel dynamic pressure, RPR, angle of attack, and angle of sideslip are shown in figures 7-10. The ideal thrust values were calculated from measurements taken on pressure and temperature rakes located at the left-hand fuselage augmentor diffuser exit as shown in figure 6. The individual thrust values were computed from exit velocities assuming an isentropic expansion to ambient pressure, and these values were area-weighted to obtain total thrust.

A list of the basic aerodynamic data in the report is shown in table 3. The longitudinal characteristics of the model for $\delta_f = 0°$ are shown in figures 11 through 13. Power-off characteristics are shown in figure 11 with the wing-root-augmentor inlet and diffuser door closed and with the horizontal tail off. The effect of operating the wing root augmentor at a DAR of 1.6 and the wing augmentor with the horizontal tail off and on is shown in figures 12(a) and 12(b), respectively. The effect of operating the wing root augmentor at a DAR of 1.0 with 26 nozzles blanked off is shown in figure 13.

The longitudinal characteristics of the model with $\delta_f = 30"$ are shown in figures 14 through 17. The effect of power off with the wing root-augmentor inlet and diffuser door closed is shown in figures 14(a) and 14(b) with the horizontal tail off and on, respectively. Figures 15 and 16 show the effect of operating the wing root augmentor at a DAR of 1.6 and 1.0, respectively. The effect of operating the wing root augmentor at a DAR of 1.0 with 26 nozzles blanked off is shown in figure 17.

The longitudinal characteristics of the model with $\delta_f = 60"$ are shown in figures 18 and 19. The effect of operating the wing root augmentor at a DAR of 1.6 with the horizontal tail off and on is shown in figures 18(a) and 18(b), respectively. Figures 19(a), 19(b), and 19(c) show the effect of operating the wing root augmentor with a DAR of 1.0 at full-nozzle thrust, 3/4-nozzle thrust, and 1/2-nozzle thrust, respectively.

The longitudinal characteristics of the model with $\delta_f = 90"$ are shown in figure 20.

The variations of C_L, C_D, C_m with $(C_J)_{aug}$ are shown in figures 21-24 for corresponding $\delta_f = 0°$, 30°, 60°, and 90°.

The variations of C_L, C_D, and C_m with angle of sideslip are shown in figures 25 through 30. Figure 25 shows these variations for $\delta_f = 0"$ at au = 0° with the augmentor operating. The effect of power off with the wing root augmentor inlet and the diffuser door closed is shown in figure 26 for $\delta_f = 30"$. The effect of the wing root augmentor operating at a DAR of 1.6 and 1.0 at $\delta_f = 30"$ is shown in figures 27 and 28, respectively. Figures 29 and 30 show this effect at $\delta_f = 60"$ and 90°, respectively, at a DAR of 1.6.

REFERENCES

1. Lummus, J. R.: Study of Aerodynamic Technology for a V/STOL Fighter/Attack Aircraft, vol. I. NASA CR-152128, 1978.

2. Aiken, Thomas N.: Thrust Augmentor Application for STOL and V/STOL. AIAA Paper 77-605, AIAA/NASA Ames V/STOL Conference, June 1977.

3. Garland, D. B.; and Whittley, D. C.: Phase 1 Wind Tunnel Tests of the 5-97 Powered, External Augmentor V/STOL Model. NASA CR-152255, 1979.

TABLE 2.- GEOMETRY OF WING AUGMENTOR

Parameters	Inboard	Middle	Outboard
Bay spans	61.6 cm (24.25 in.)	57.8 cm (22.75 in.)	57.1 cm (22.5 in.)
Nozzle area/bay	31.5 cm^2 (4.88 $in.^2$)	24.1 cm^2 (3.73 $in.^2$)	18.6 cm^2 (2.88 $in.^2$)
Total nozzle area/bay span, $\bar{t}$	0.201	0.16[illegible]	0.128 in.
Number of nozzles (N)	15	17	22
Area per nozzle (A_N)	2.10 cm^2 (0.325 $in.^2$)	1.41 cm^2 (0.219 $in.^2$)	0.85 cm^2 (0.131 $in.^2$)
Pitch (p)	4.06 cm (1.60 in.)	3.35 cm (1.32 in.)	2.57 cm (1.01 in.)
Nozzle span (b)	9.17 cm (3.61 in.)	7.52 cm (2.96 in.)	5.82 cm (2.29 in.)
Nozzle thickness (t)	0.23 cm (0.090 in.)	0.19 cm (0.074 in.)	0.14 cm (0.057 in.)
Nozzle aspect ratio (AR)	40	40	40
Throat (mid span) (L_T)	10.59 cm (4.17 in.)	8.64 cm (3.40 in.)	6.73 cm (2.65 in.)
Exit (mid span) (L_E)	16.94 cm (6.67 in.)	13.82cm (5.44 in.)	10.77 cm (4.24 in.)
Diffuser area ratio L_E/L_T	1.60	1.60	1.60
Nozzle inlet area/exit area	5.0	5.0	5.0
Augmentor length (mid span) (L)	43.9 cm (17.3 in.)	37.3 cm (14.7 in.)	30.7 cm (12.1 in.)
$L/\bar{t}$	86	90	95

Total	
Span (per wing)	176.5 cm (69.5 in.)
Nozzle area (per wing)	74.2 cm^2 (11.5 $in.^2$)

TABLE 2 — LIST OF BASIC DATA FIGURES

Figure	δ_f, deg	δ_j, deg: Fuselage	δ_j, deg: Wing	α, deg	M	T_t, lb	T_t, lb	i_t, deg	DAR	RPR	Wing root augmentor exit rake	Remark
	0	0	0	-10 to 20		703.8	14.7	Off	None	1.0	Off	Clean configuration with wing root augmentor inlet closed and diffuser door closed (see figs. 1(a) and 1(b)) Power off.
		3.48 1.74 1.16 .70	0.92 .46 .31 .19	10 to 20 -8 to 16 -8 to 16 -8 to 16		234.6 469.2 708.6 1163.5	4.9 9.8 14.8 24.3		1.6	2.3		
		1.74 1.17 .70	0.46 .31 .19	-10 to 26 -10 to 20		469.2 699.0 1158.7	9.8 14.6 24.2	15 15 15				
		0.61 .36 .23	0.31 .19 .12	-8 to 12 -8 to 12 -8 to 12		708.6 1168.3 1857.7	14.8 24.4 38.8	Off	1.0		Off	1/2-thrust output. Thirteen nozzles of wing root augmentor per side blanked off
14(a)	30	0	0	-10 to 20		694.3	14.5		None	1.0		Clean configuration. Power off.
14(b)		0	0			699.0	14.6	15 & 15	None	1.0		
15		3.53 1.76 1.17	0.84 .47 .31			234.6 469.2 703.8	4.9 9.8 14.7	Off	1.6	2.3		
16		1.78 1.19 .71 .44	0.47 .31 .19 .12	10 to 10		469.2 699.0 1163.5 1857.7	9.8 14.6 24.3 38.8		1.0			
17		0.61 .37 .23	0.31 .19 .12	-8 to 12		699.0 1168.7 1863.4	14.6 24.2 38.5					1/2-thrust output; 13 nozzles of wing root augmentor per side blanked off.
18(a)	40	3.52 1.76 1.18	0.94 .47 .31	-10 to 20		234.6 464.4 703.8	4.9 9.7 14.7		1.6		On	
18(b)		3.53 1.76 1.18	0.94 .47 .31	-8 to 26 -10 to 26 -10 to 26		234.6 469.2 708.6	4.9 9.8 14.8	15				

TABLE 3.- CONCLUDED.

Figure	δ_f, deg	C_J Fuselage	C_J Wing	α_v, deg	β, deg	q, N/m^2	q, lb/ft^2	i_t, deg	DAR	RPR	augmentor exit	Remark
19(a)	0	3.66	0.97	-10 to 20	0	229.8	4.8	0	1.0	2.3	On	
		1.80	.48			464.4	9.7					
		1.18	.31			703.8	14.7					
		.71	.19			1163.5	24.3					
19(b)		0.37	0.31	-10 to 20		708.6	14.8					3/4-thrust output; 17 nozzles of wing root augmentor per side blanked off.
		.33	.19	-10 to 12		1163.5	24.3					
		.33	.12	-10 to 12		1853.0	38.7					
19(c)		0.91	0.47	-10 to 20		469.2	9.8					1/2-thrust output; 13 nozzles of wing root augmentor per side blanked off.
		.61	.31	-10 to 20		703.8	14.7					
		.37	.19	-10 to 20		1168.3	24.4					
20	30	6.20	1.66	-10 to 12		143.6	3.0		1.6	2.4	Off	
	30	3.85	1.04	-10 to 12		239.4	5.0			2.4		
	30	1.85	.50	-10 to 12		469.2	9.8			2.4		
21	0	1.15 to 1.63	0.31 to 0.44	0		469.2	9.8			1.8 to 222	On	Full-thrust output
	0	.15 to .65	.05 to .17			1168.3	24.4			1.2 to 222	On	Full-thrust output
	0	.53 to 2.13	.30 to 1.14			229.8	4.8		1.0	1.3 to 225	Off	1/2-thrust output
22	30	0.61 to 1.92	0.18 to 0.51			459.6	9.6		1.6	1.5 to 2.4	On	Full-thrust output
		.86 to 1.89	.24 to .50			464.4	9.7		1.0	1.5 to 2.4	Off	Full-thrust output
		.20 to .75	.06 to .20			1163.5	24.3			1.3 to 2.4	Off	Full-thrust output
		.26 to 1.04	.15 to .54			469.2	9.8			1.3 to 2.5	On	1/2-thrust output
		.11 to .41	.06 to .21			1168.3	24.4			1.3 to 2.5	On	1/2-thrust output
23	60	0.59 to 1.65	0.17 to 0.44			474.0	9.9		1.6	1.3 to 2.2	On	
24	30	0.8 to 3.50	0.26 to 0.90			229.8	4.8			1.2 to 2.2	Off	
		.3 to 1.31	.17 to .51			469.2	9.8			1.3 to 2.4	Off	
25	0	0.83	0.23		-12 to 12	474.0	9.9			1.5	On	
	0	1.74	.46			474.0	9.9			2.3	On	
26	30	0	0	0 & 0.02		699.0	14.6		None	1.0	Off	Clean configuration with wing root augmentor inlet covered and diffuser door closed.
27		0.81	0.22	0		469.2	9.8		1.6	1.5	On	
		1.74	.46			469.2	9.8		1.6	2.3	On	
28		0.31	0.23			469.2	9.8		1.0	1.5	Off	
29	60	0.80	0.22			464.4	9.7		1.6	1.5	On	
		1.76	.47			464.4	9.7			2.3	On	
30	30	3.54	0.34		0 to 16	234.6	4.9			2.3	Off	
		1.83	.09		0 to 16	459.6	9.6			2.3	Off	

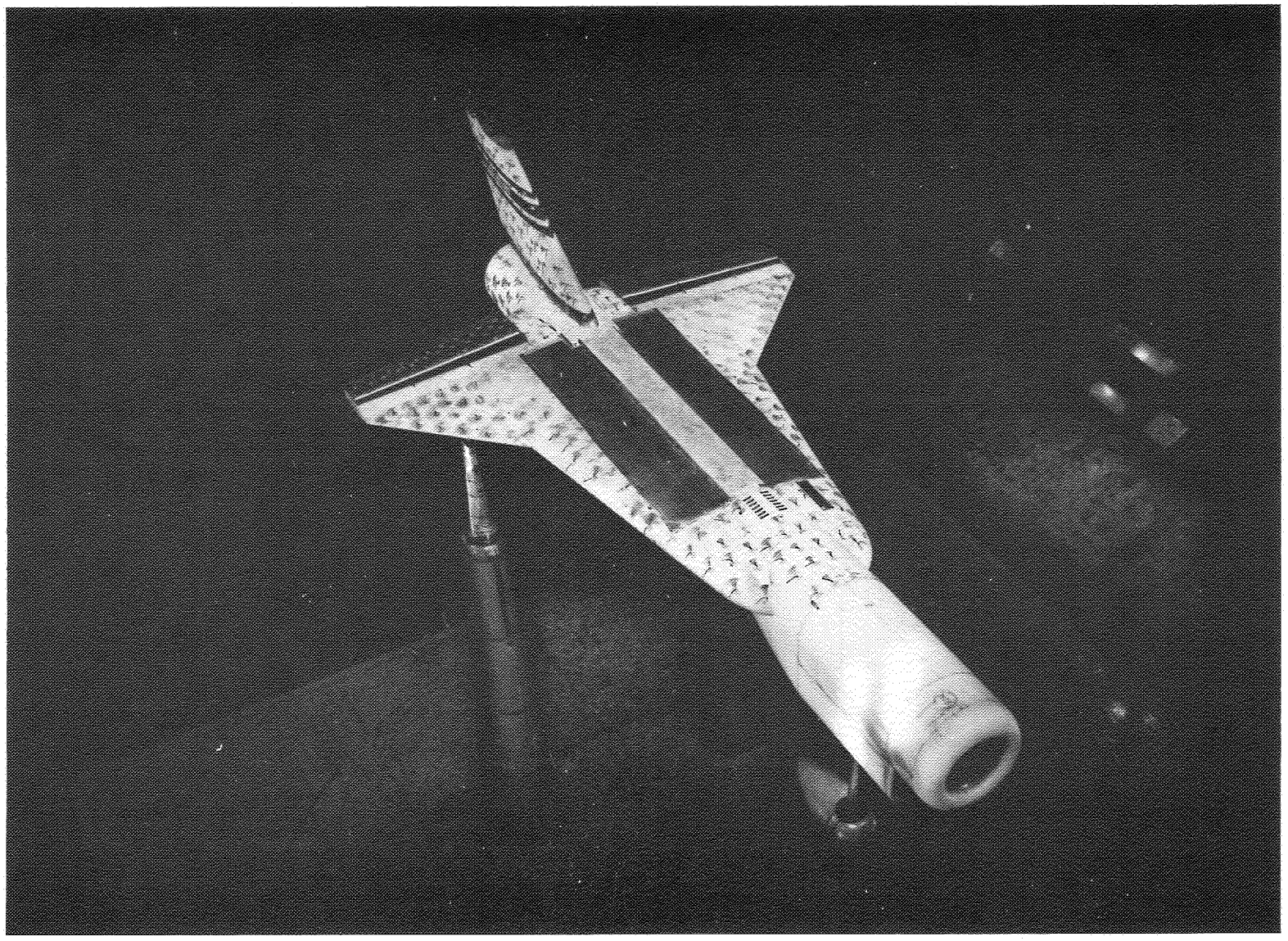

(a) Overhead view with wing root-augmentor inlet closed.

Figure 1.- Photographs of the model as mounted in the Ames 40- by 80-Foot Wind Tunnel.

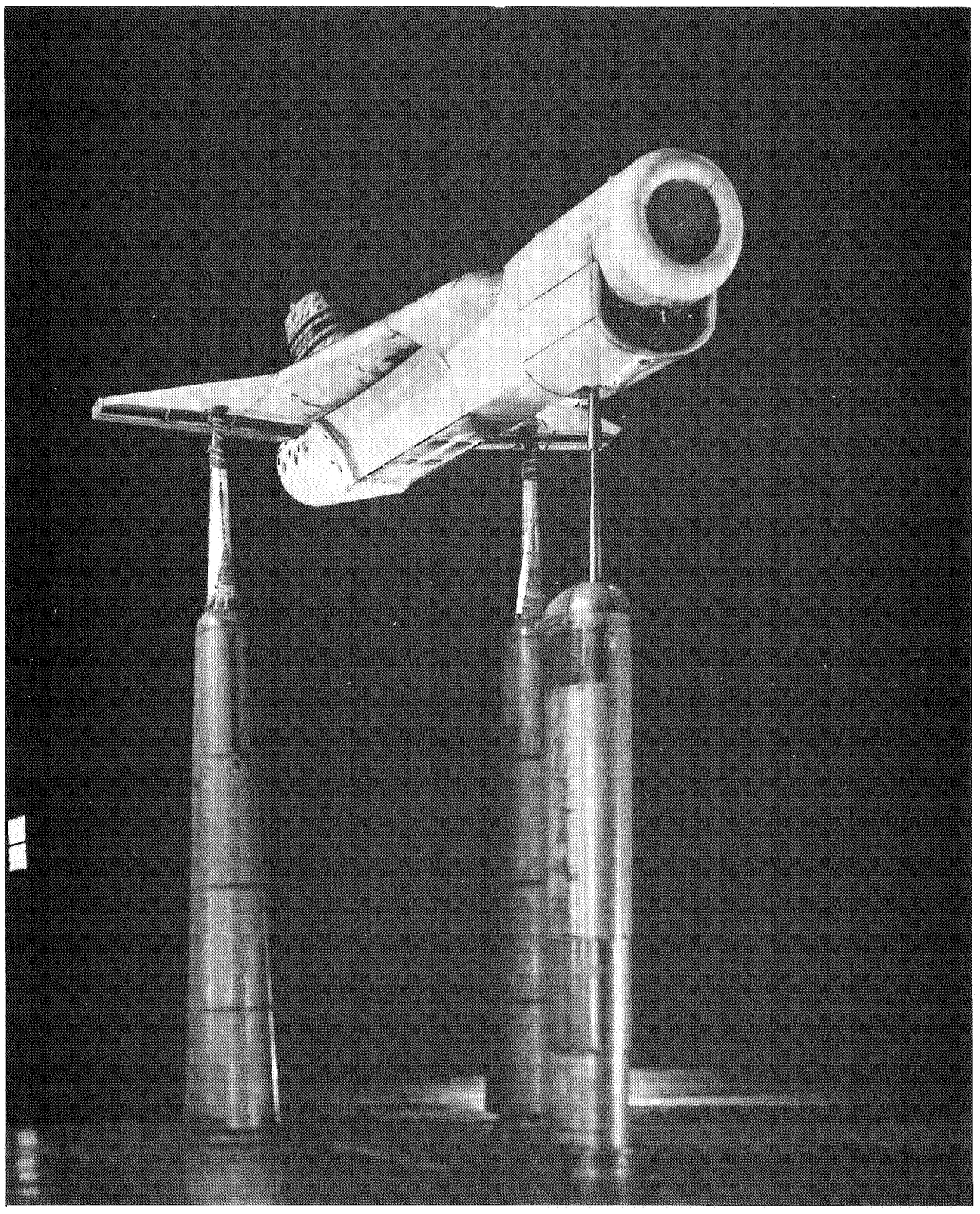

(b) 3/4-front view of model with wing root-augmentor door closed.

Figure 1.- Continued.

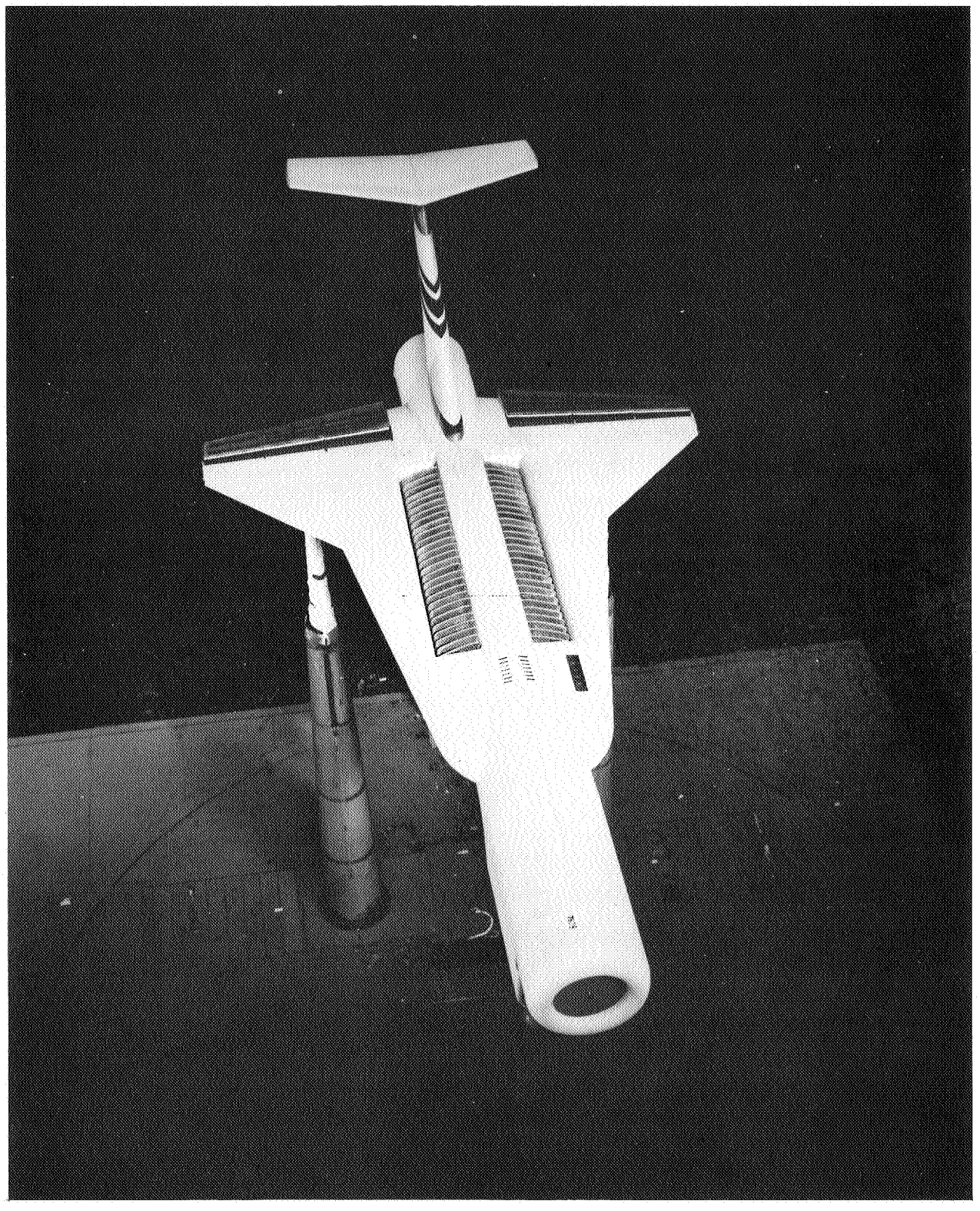

(c) Overhead view of model showing wing root augmentor.

Figure 1.- Continued.

(d) 3/4-front view of model showing wing root-augmentor diffuser with end plates (outboard diffuser door removed).

Figure 1.- Concluded.

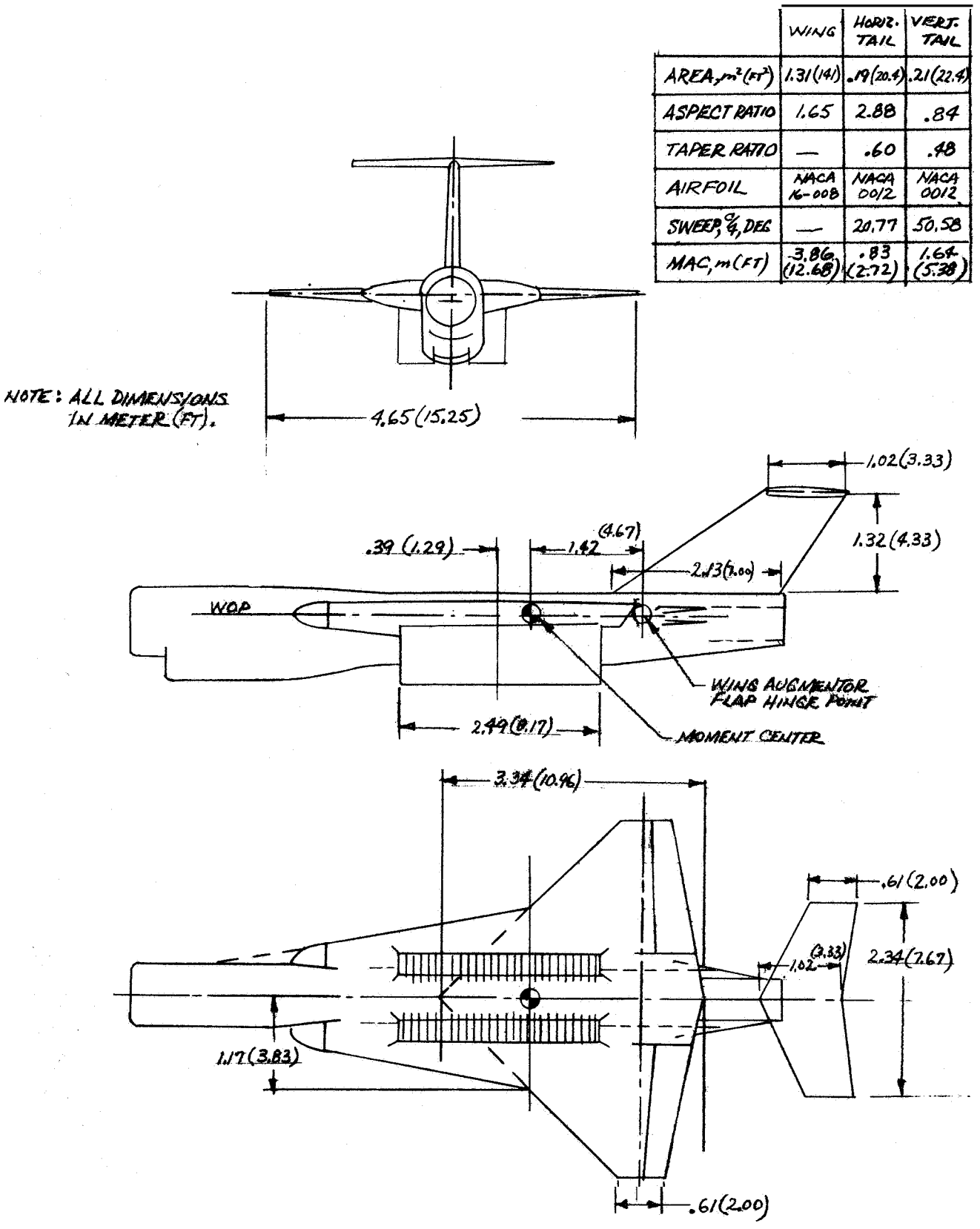

(a) 597 powered external augmentor VTOL model.

Figure 2.– Geometric details of the model.

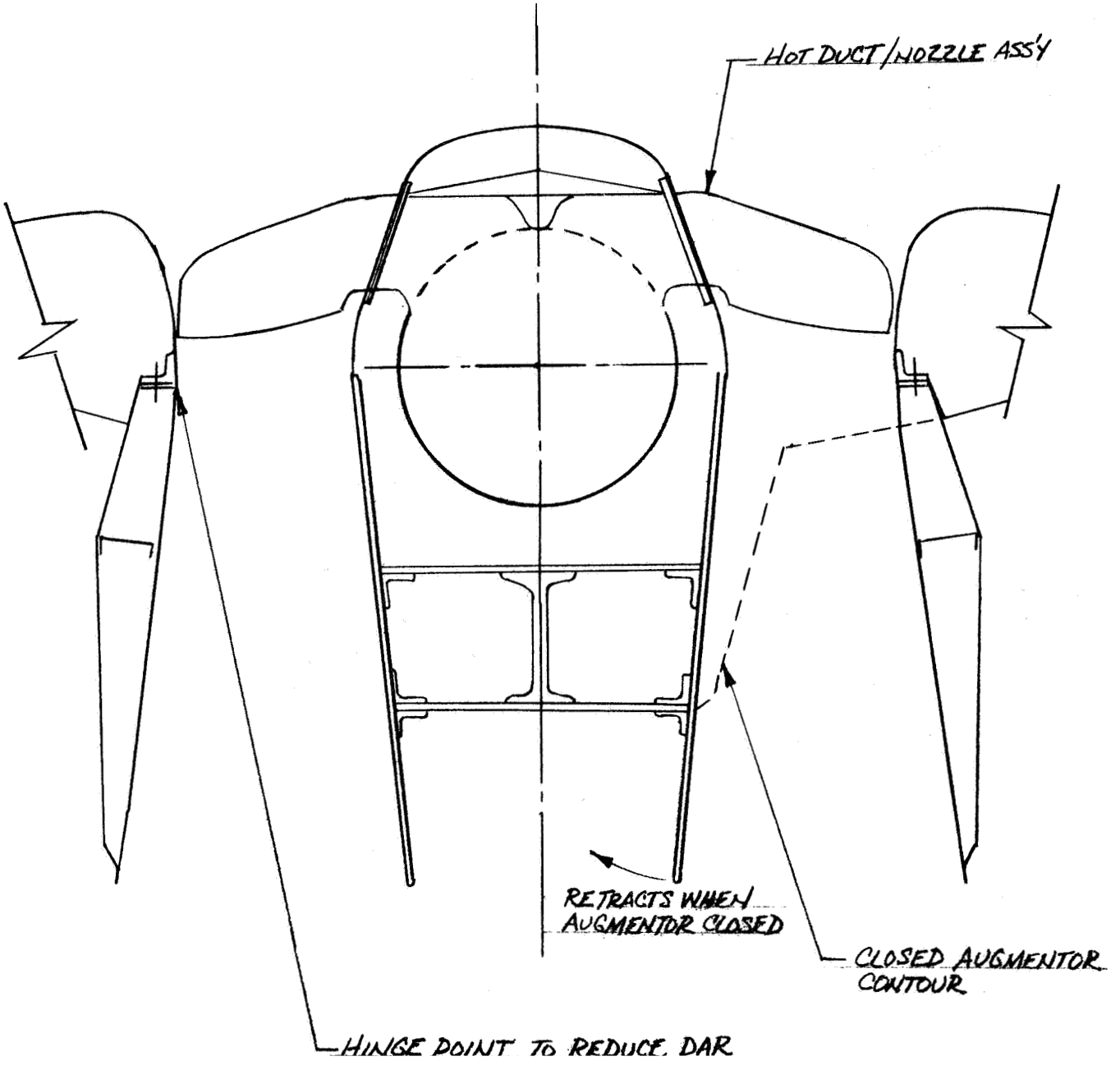

(b) Section through wing root augmentor.

Figure 2.– Continued.

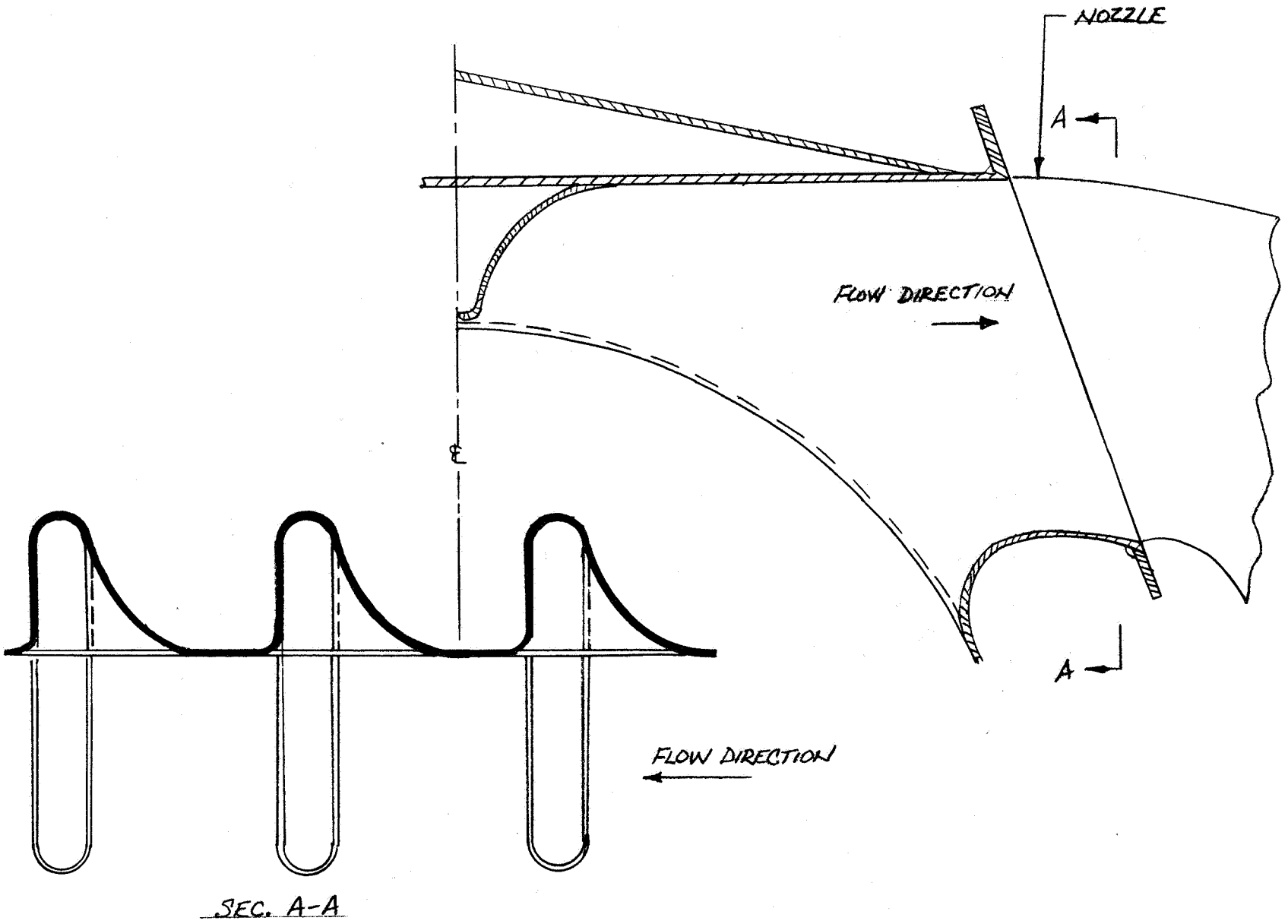

(c) Wing root augmentor nozzle takeoffs.

Figure 2.- Continued.

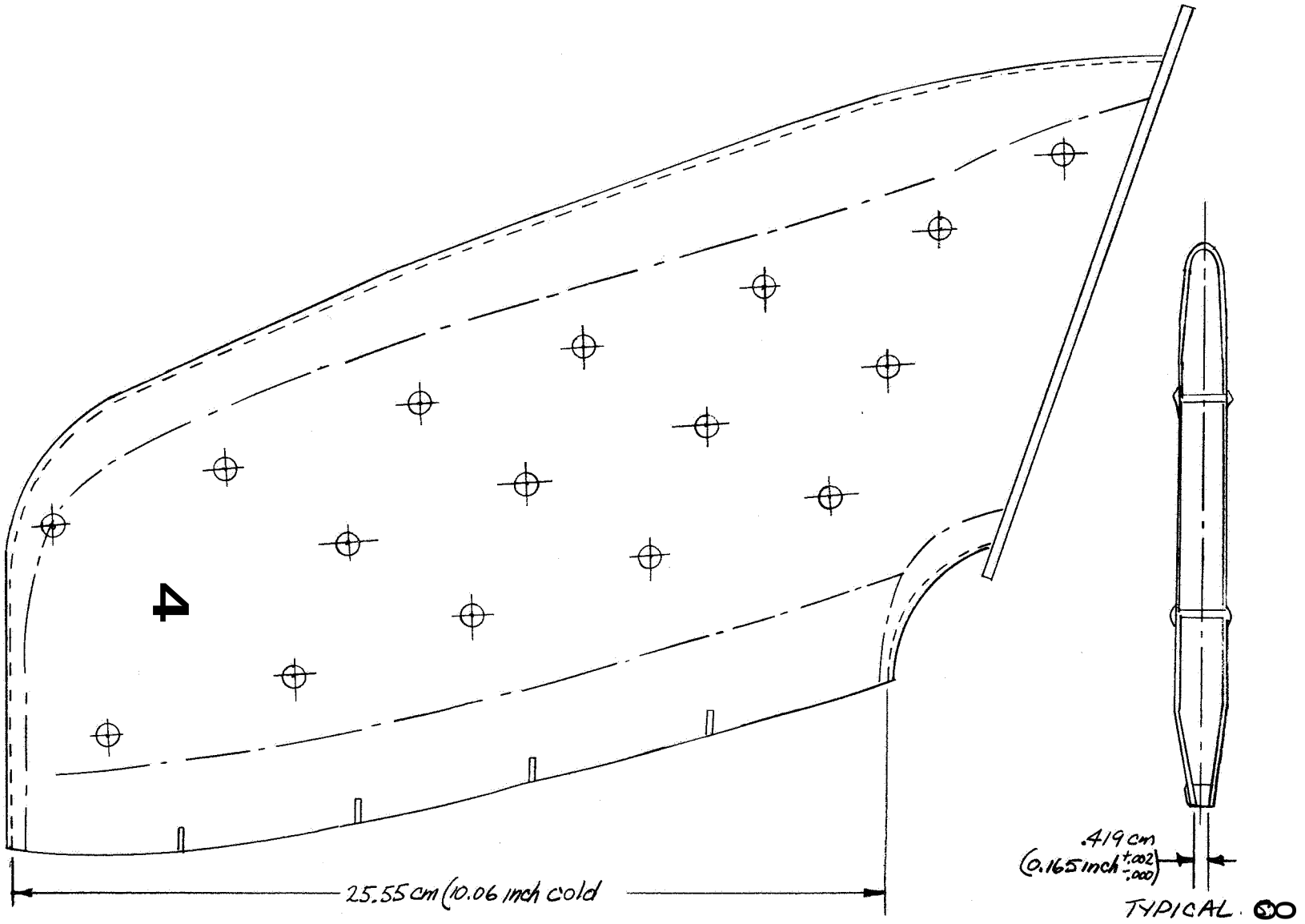

(b) Wing root augmentor nozzle

Figure 2 - Continued

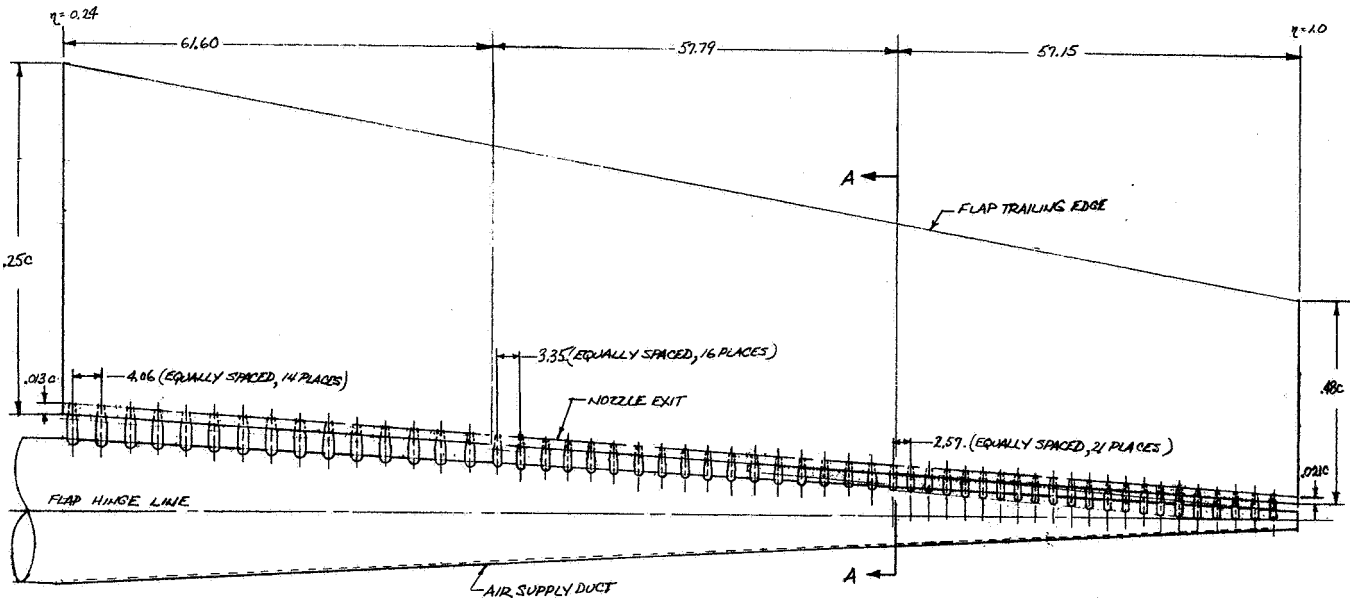

PLAN VIEW

NOTE: ALL DIMENSIONS IN CM. EXCEPT AS NOTED.

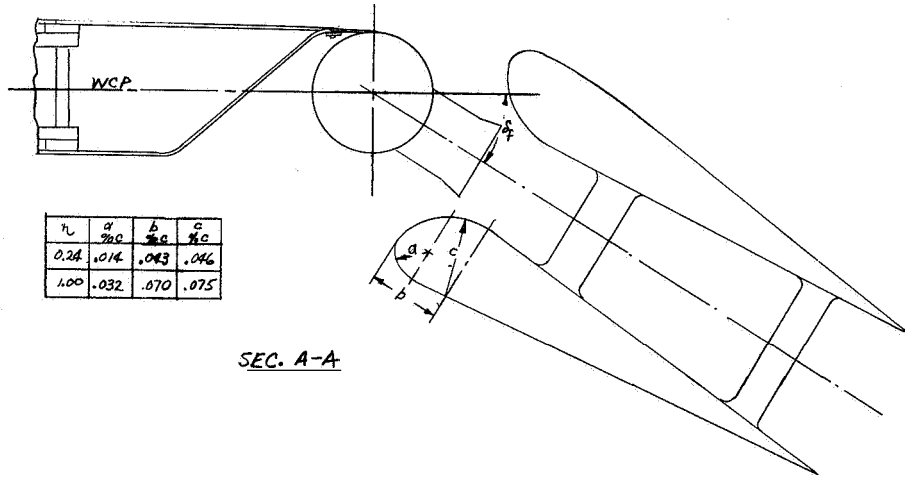

η	a %c	b %c	c %c
0.24	.014	.043	.046
1.00	.032	.070	.075

SEC. A-A

(e) Wing augmentor details.

Figure 2.– Continued.

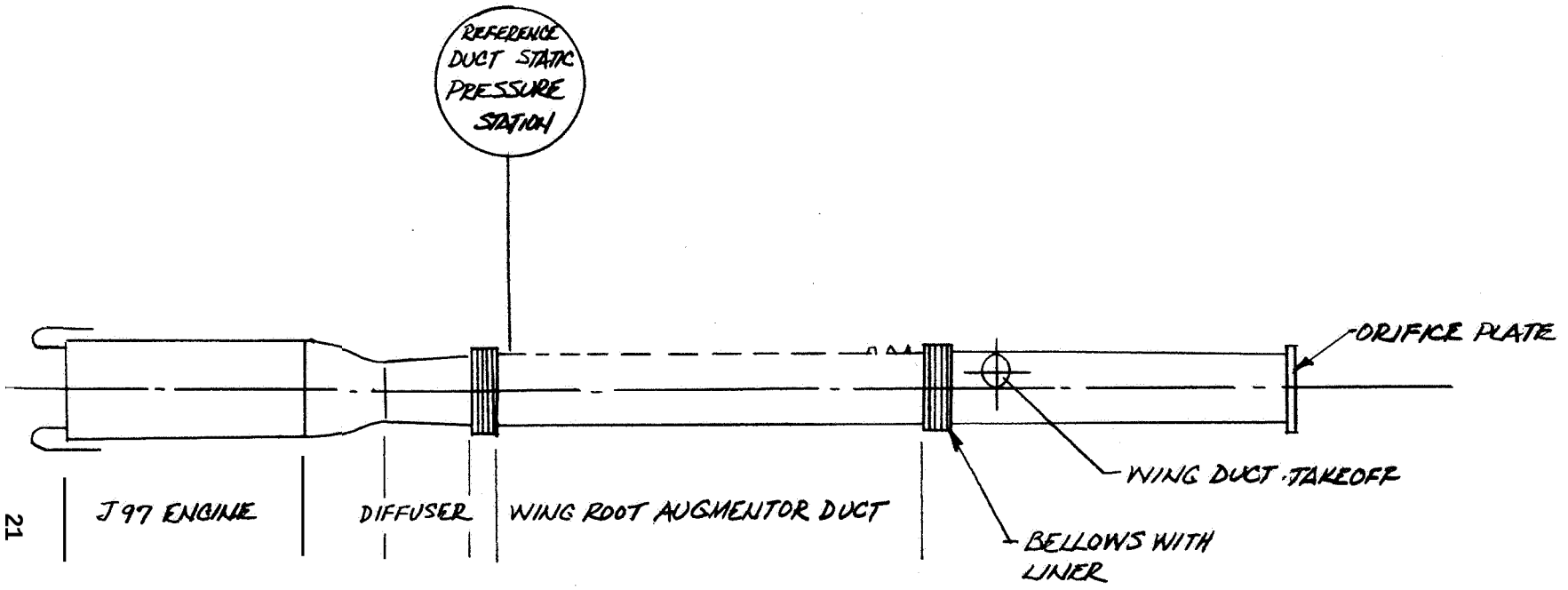

(f) Location of duct static pressure tap

Figure 2.- Concluded.

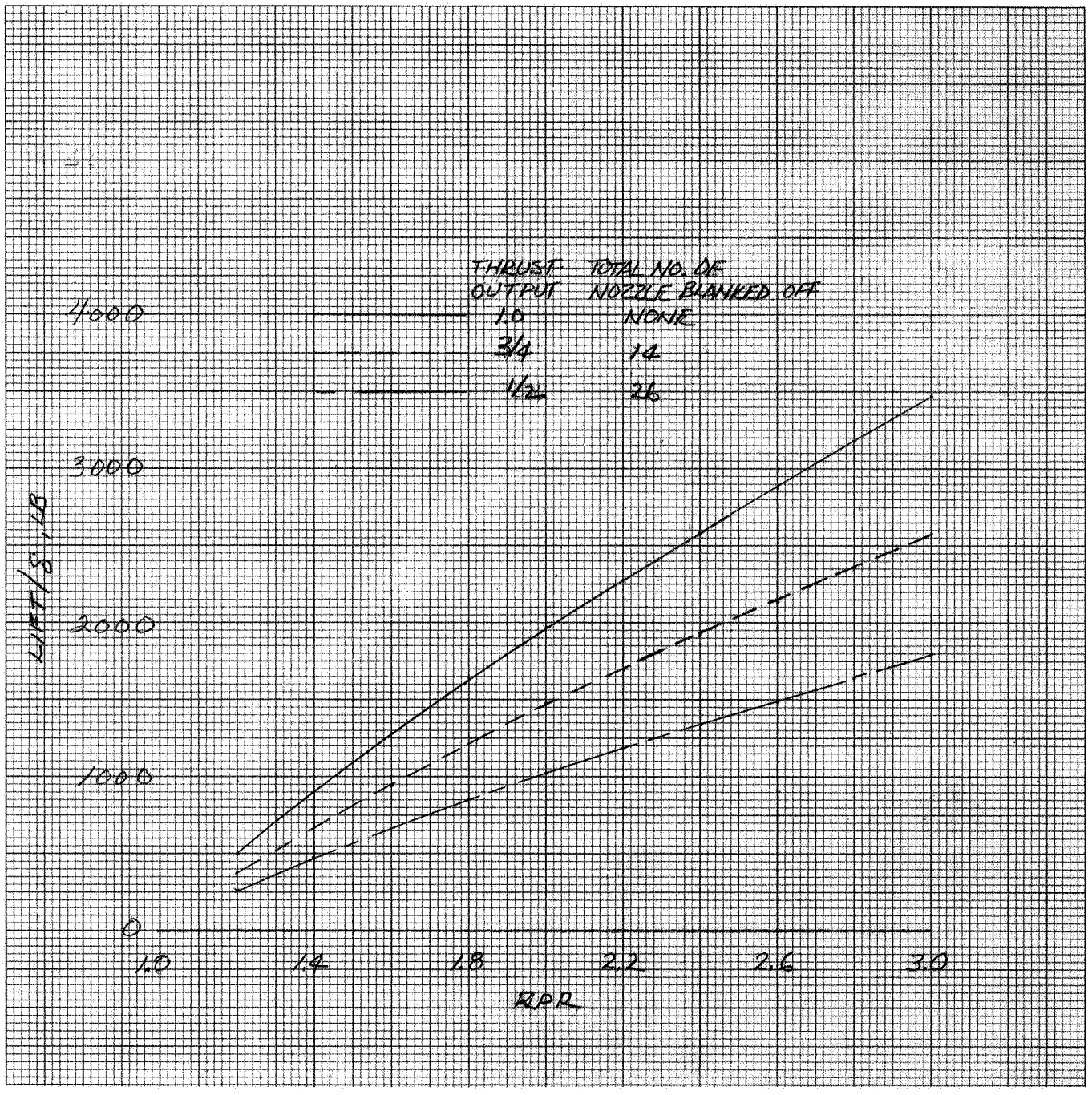

Figure 3.- Variation of wing root-augmentor primary thrust with reference duct static-pressure ratio; $\alpha = 0°$, $q = 0$ n/m^2.

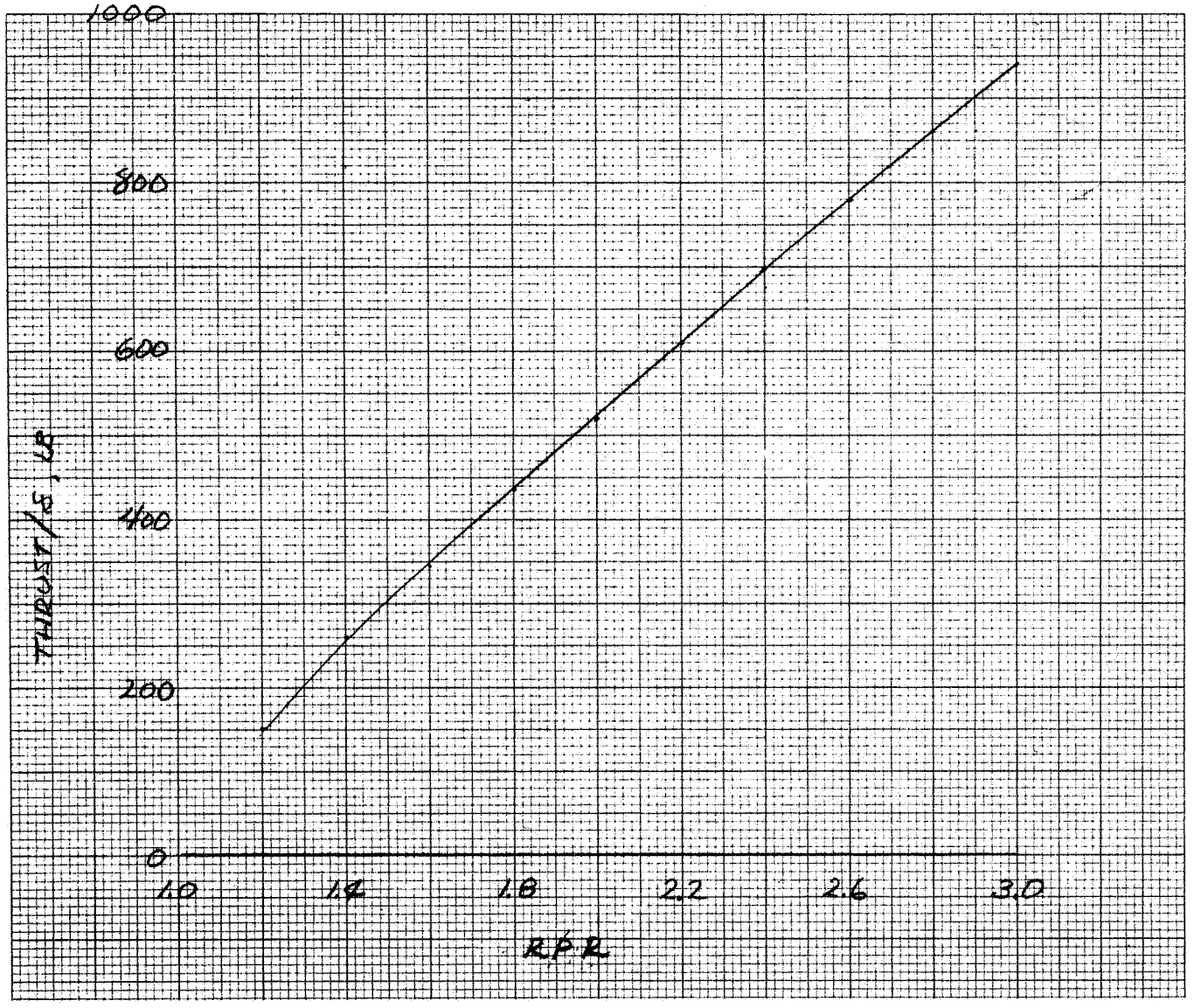

Figure 4.- Variation of calculated wing augmentor primary thrust with reference duct static pressure ratio; $\alpha = 0°$, $\delta_f = 0°$, $q = 0$ N/m^2.

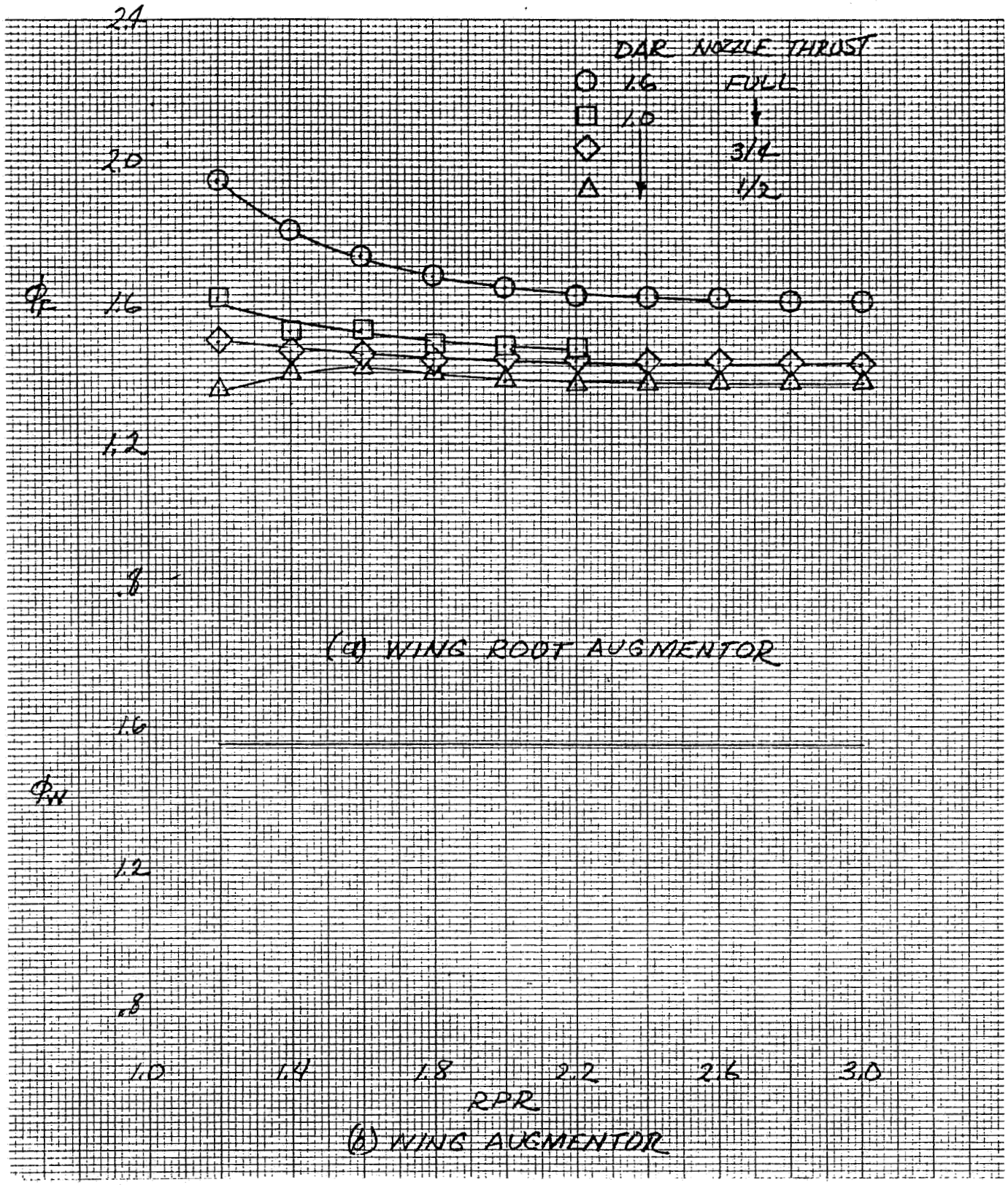

Figure 5.- Variation of gross thrust-augmentation ratio with reference duct static pressure ratio; $a = 0°$, $q = 0\ N/m^2$.

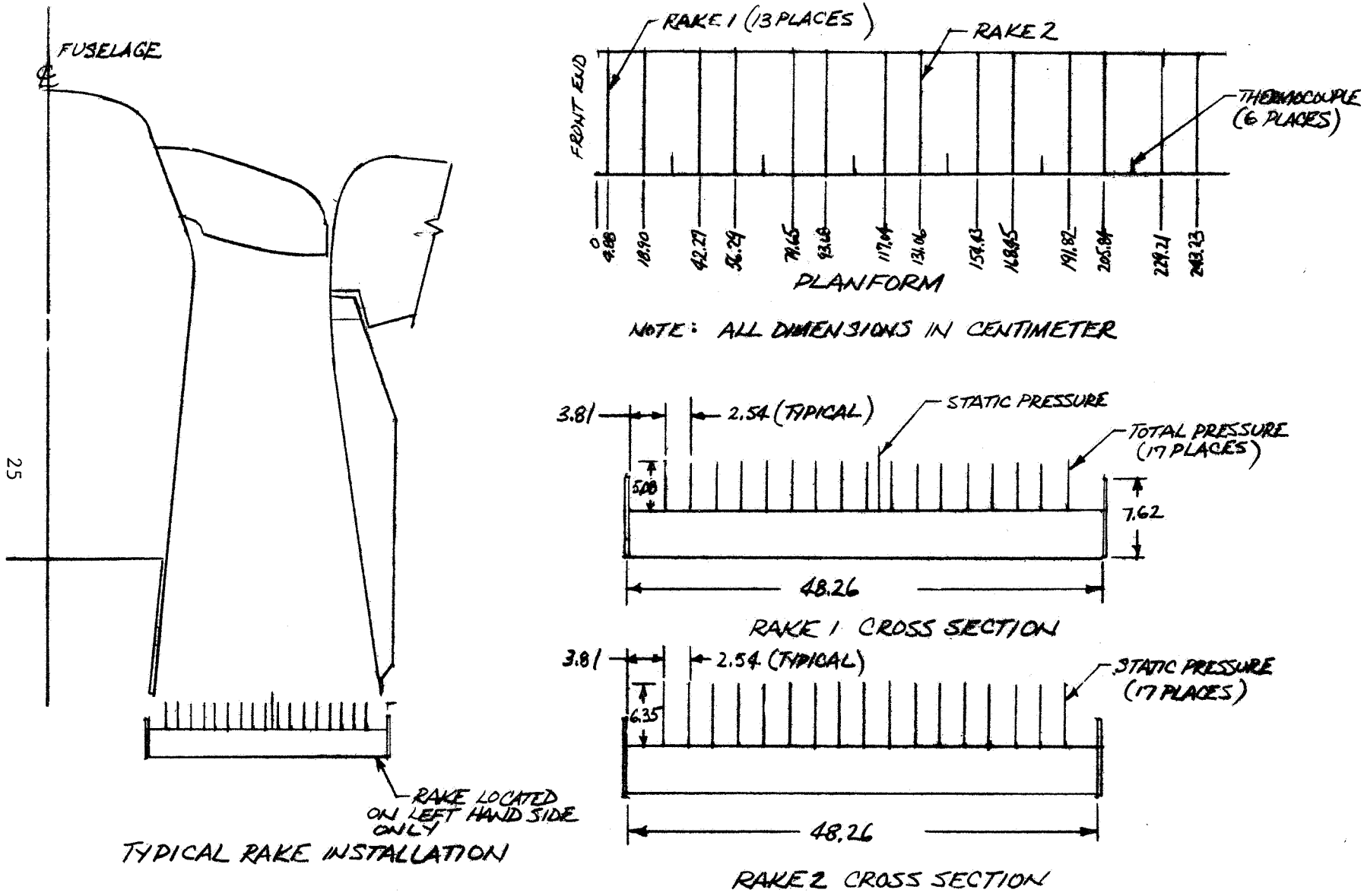

Figure 6.- Wing root-augmentor exit rake installation and details.

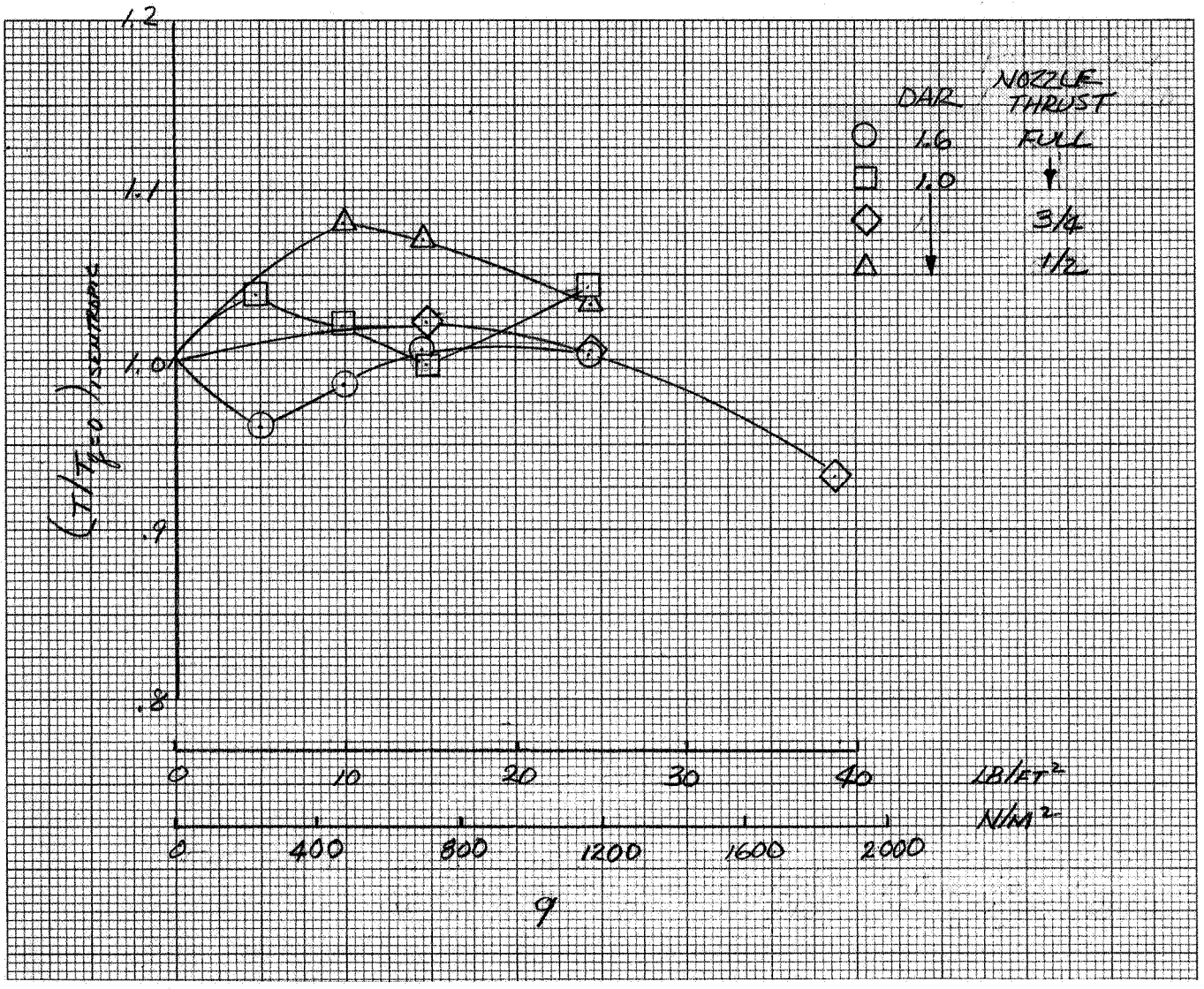

Figure 7.- Variation of ideal thrust with forward speed to ideal static-thrust ratio of wing root augmentor with wind-tunnel dynamic pressure; α_u = 0°, RPR = 2.3.

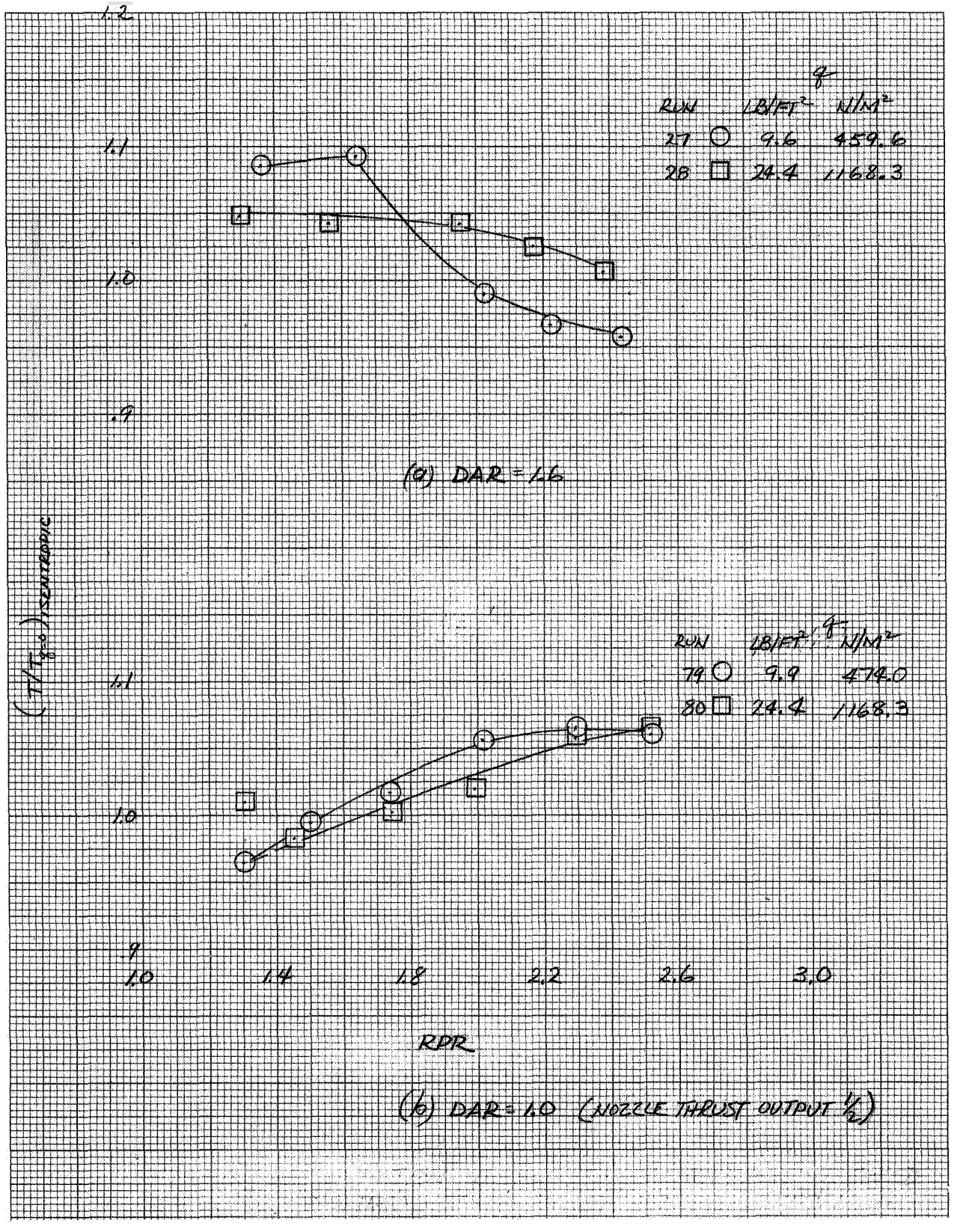

Figure 8.- Variation of ideal thrust at forward speed to ideal static-thrust ratio of wing root augmentor with reference duct static-pressure ratio; $\alpha = 0°$, $\delta_f = 30°$.

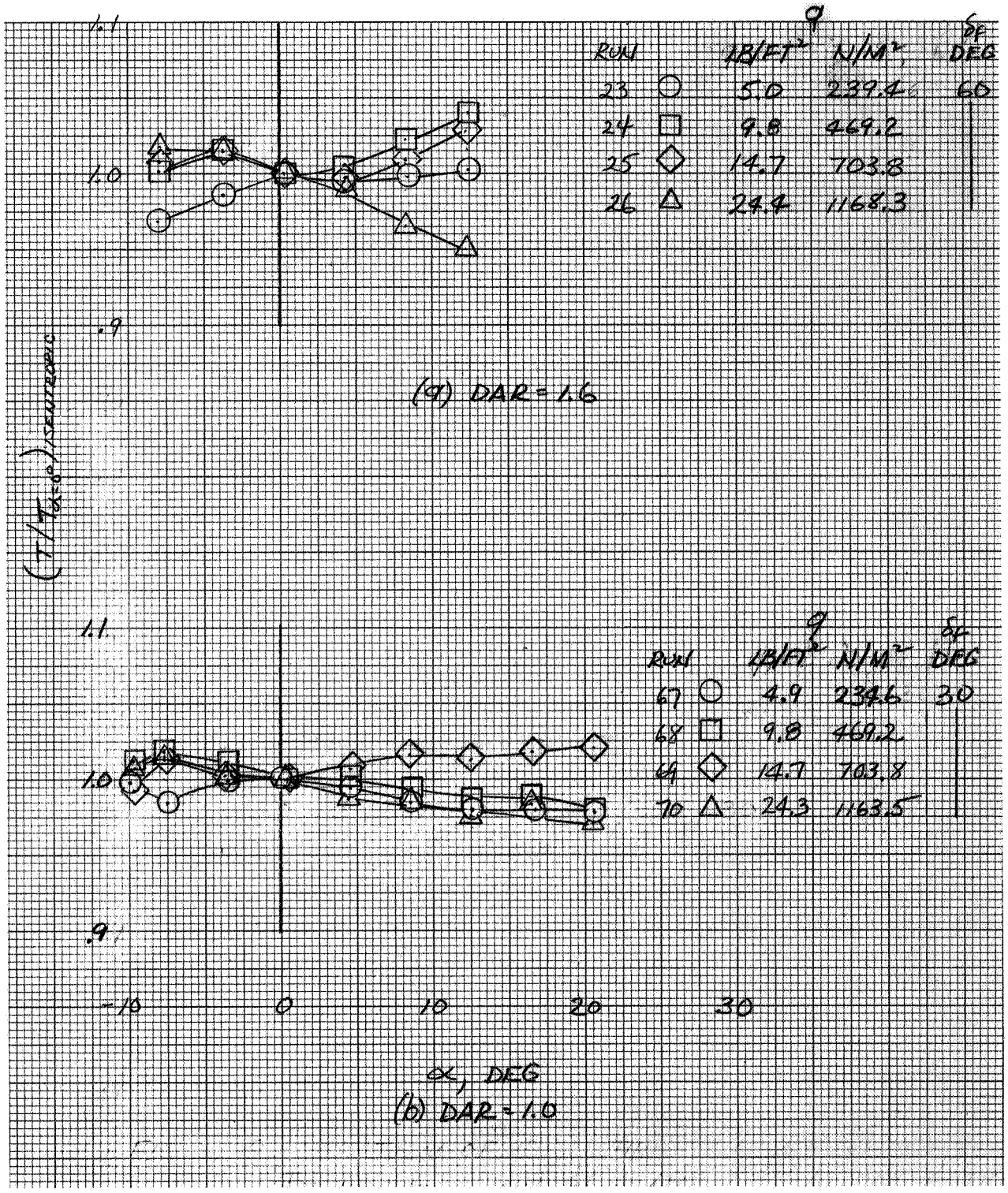

Figure 9.- Variation of ideal thrust at angle of attack to ideal thrust at zero angle-of-attack ratio of wing root augmentor; RPR = 2.3.

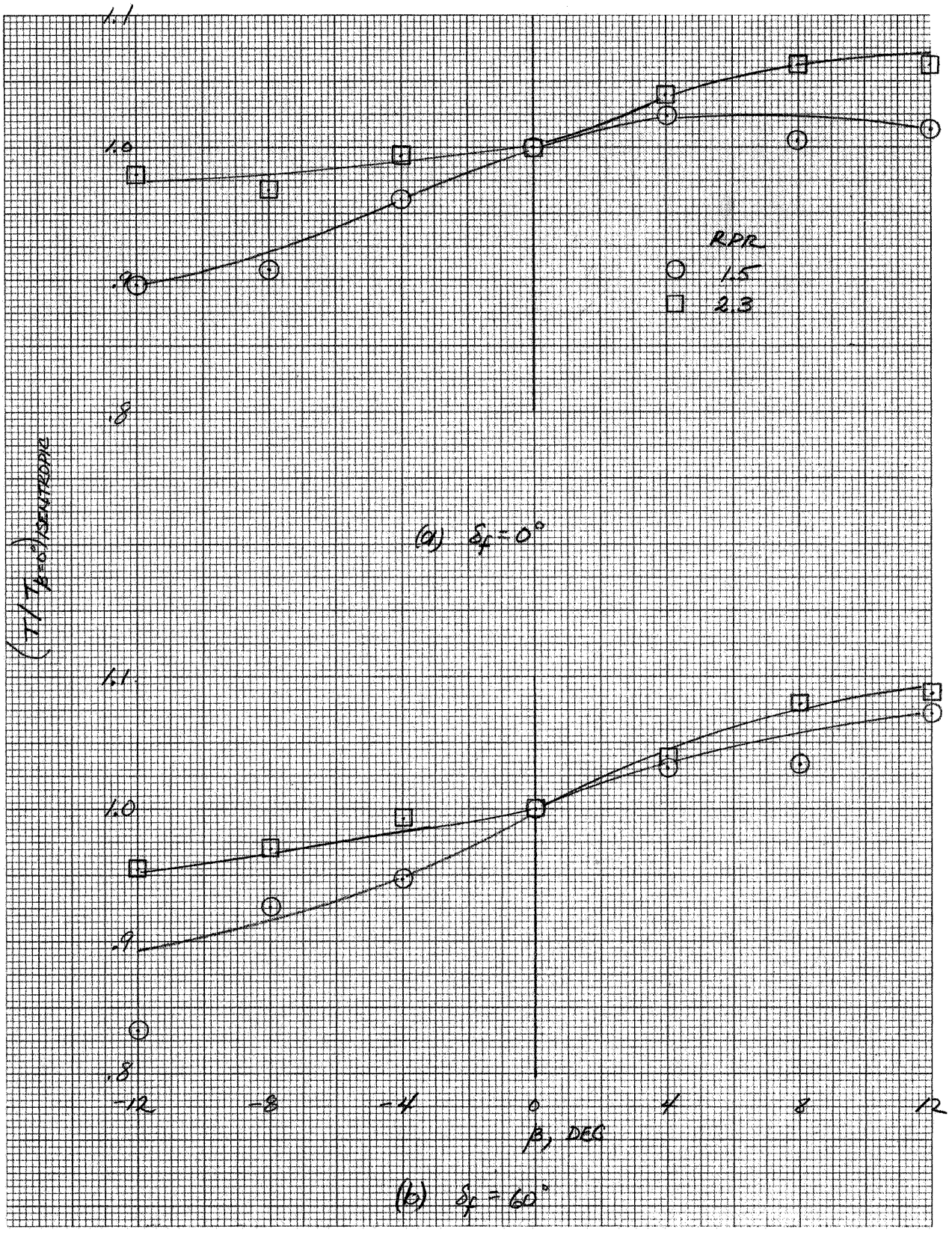

Figure 10.– Variation of ideal thrust at angle of sideslip to ideal thrust at zero angle of sideslip ratio with angle of sideslip; α_u = 0°, **q** = 479 N/m^2 (10 lb/ft^2), wing root augmentor **DAR** = 1.6.

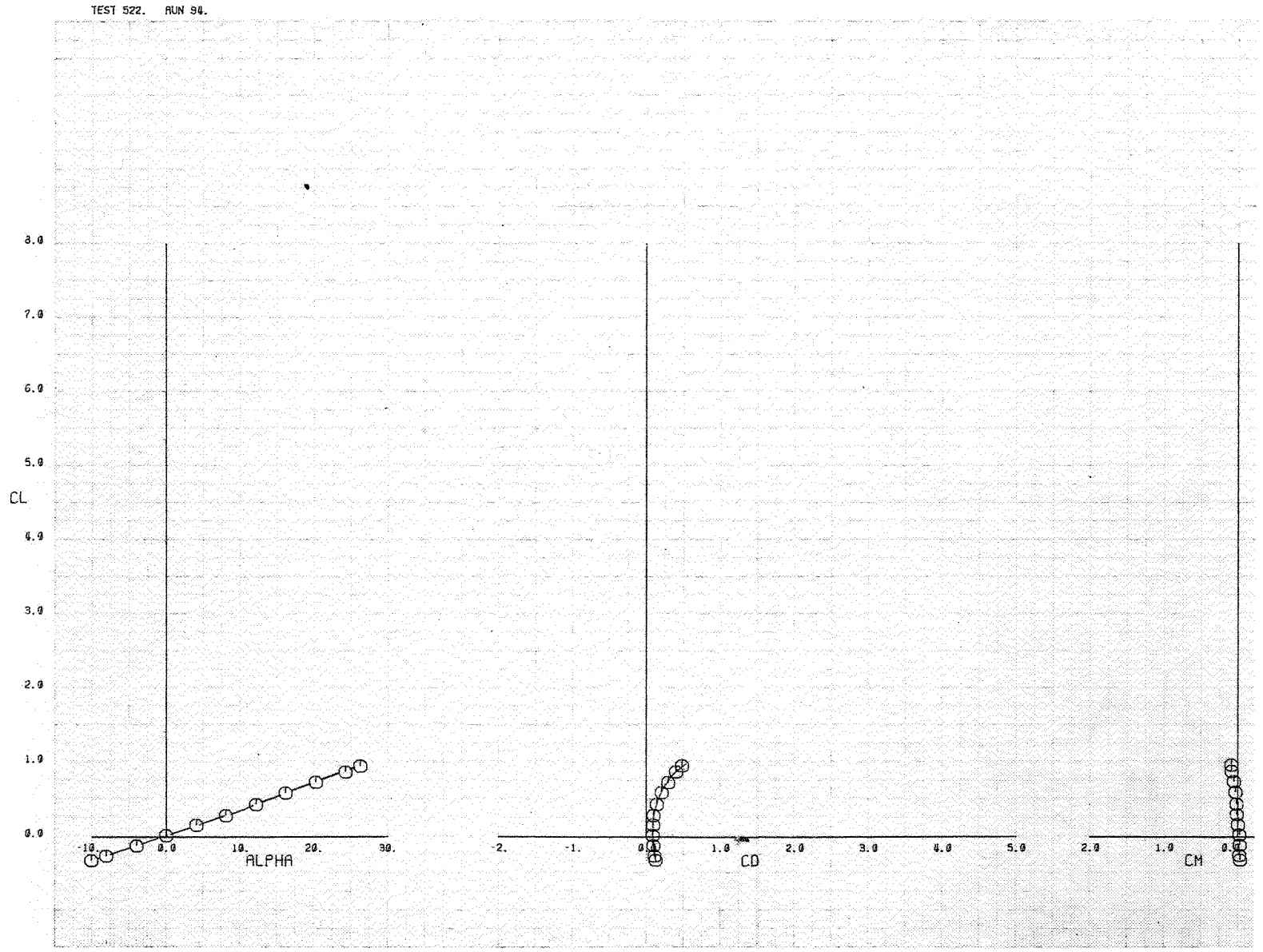

Figure 11.- Longitudinal characteristics of the model with wing root augmentor inlet and diffuser door closed; $\delta_f = 0°$, power off, $q = 703.8$ N/m^2 (14.7 lb/ft^2), wing root augmentor exit rake off, horizontal tail off.

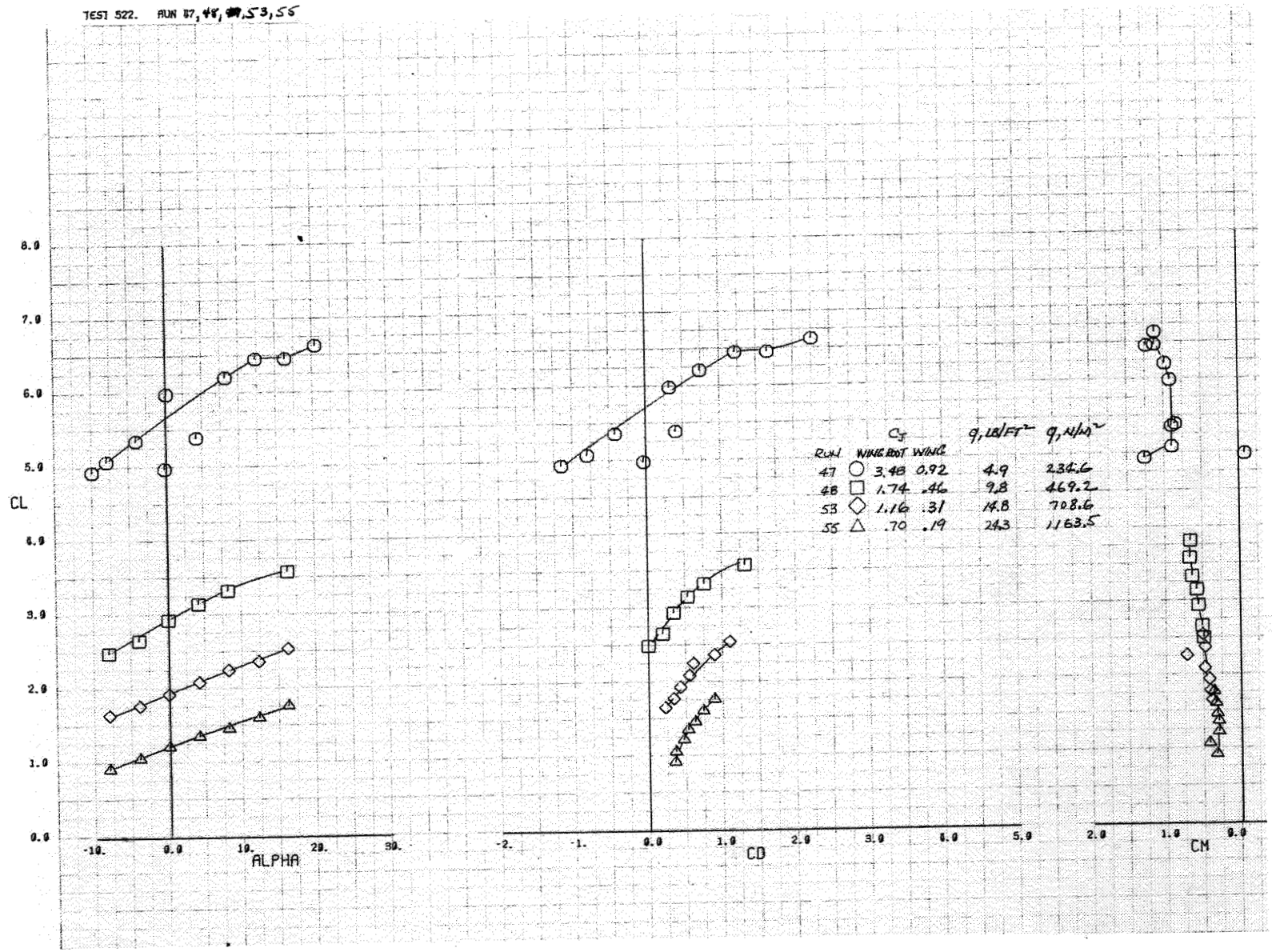

(a) Horizontal tail off.

Figure 12.- Longitudinal characteristics of the model with wing root and wing augmentors operating; δ_f = 0°, RPR = 2.3, wing root DAR = 1.6, wing root augmentor exit rake on.

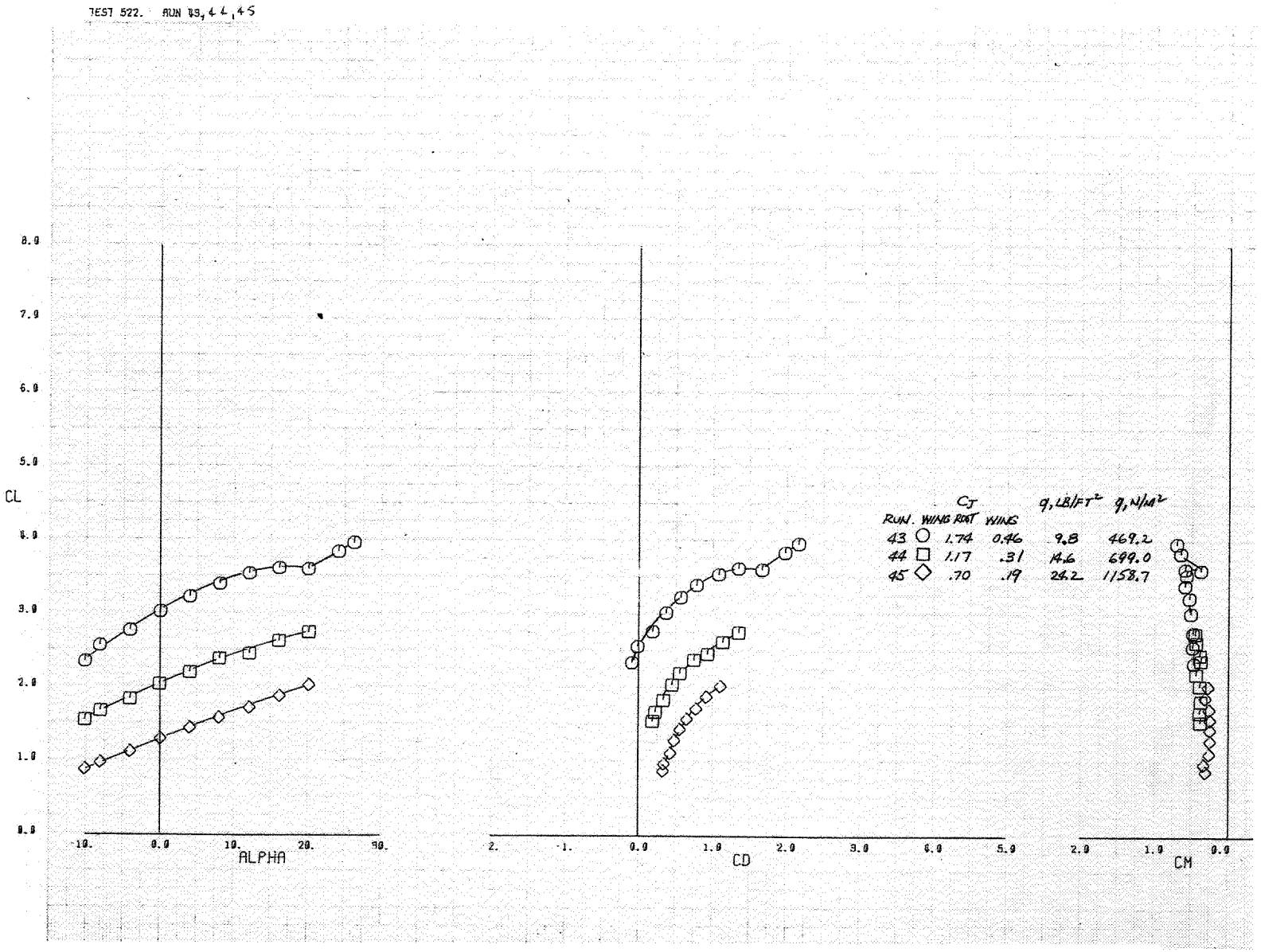

(b) $i_t = 15°$.

Figure 12.- Concluded.

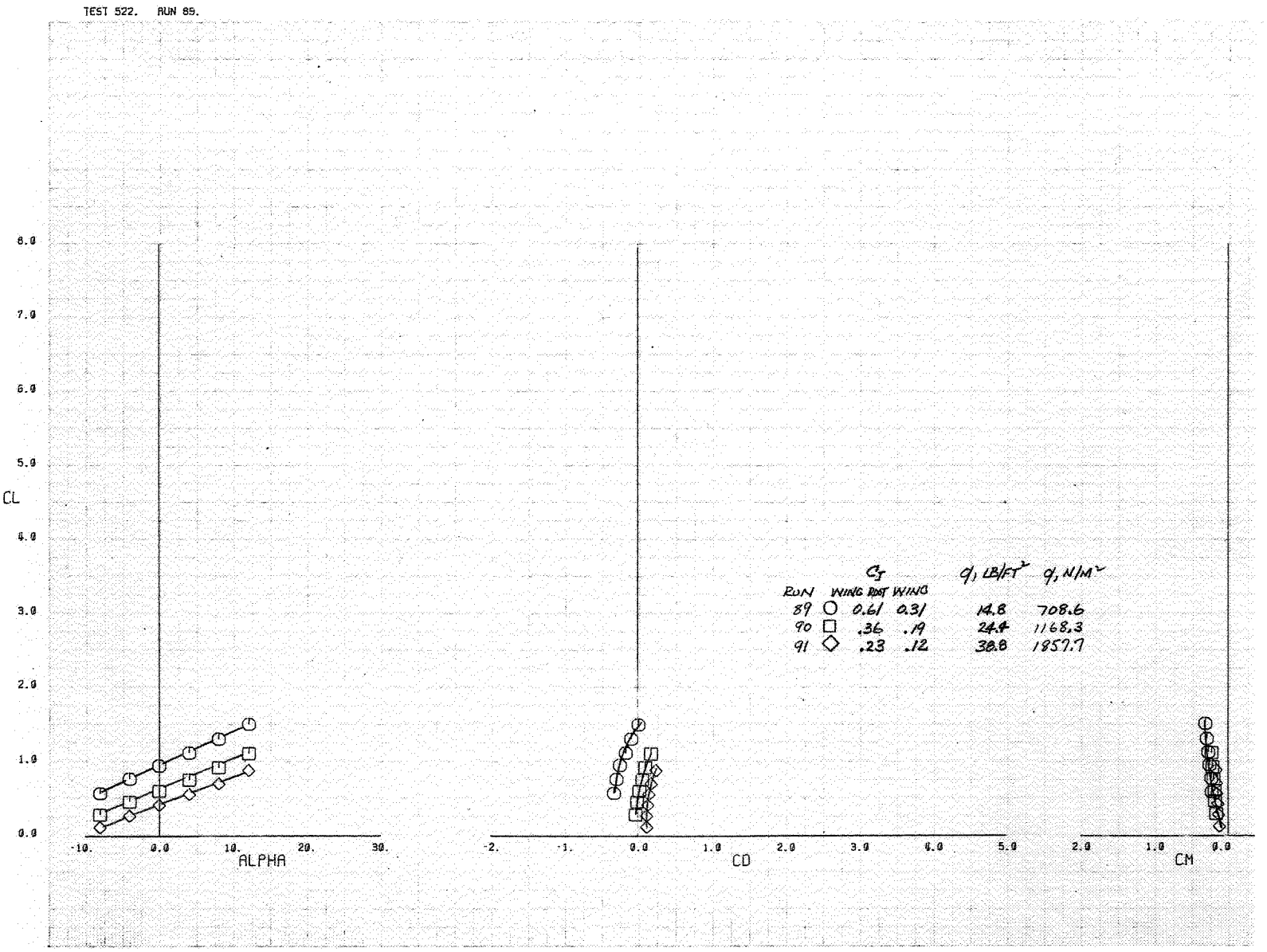

Figure 13.- Longitudinal characteristics of the model with one-half the wing root augmentor nozzle thrust; δ_f = 0°, RPR = 2.3, wing root DAR = 1.0, wing root augmentor exit rake off, horizontal tail off.

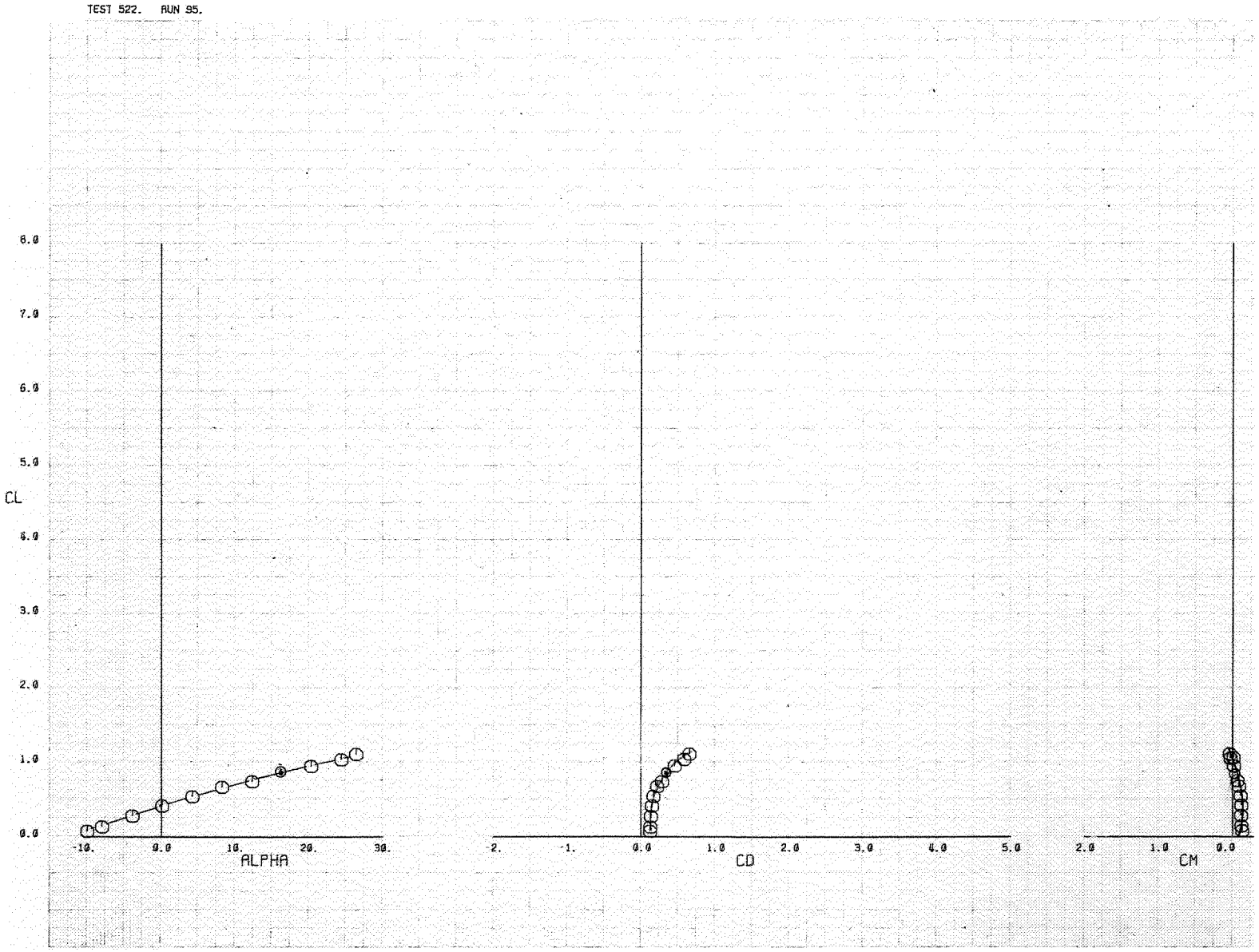

(a) Horizontal tail off, $q = 694.3\ N/m^2$ (14.5 lb/ft^2).

Figure 14.- Longitudinal characteristics of the model with wing root augmentor inlet and diffuser door closed; $\delta_f = 30°$, power off, wing root augmentor exit rake off.

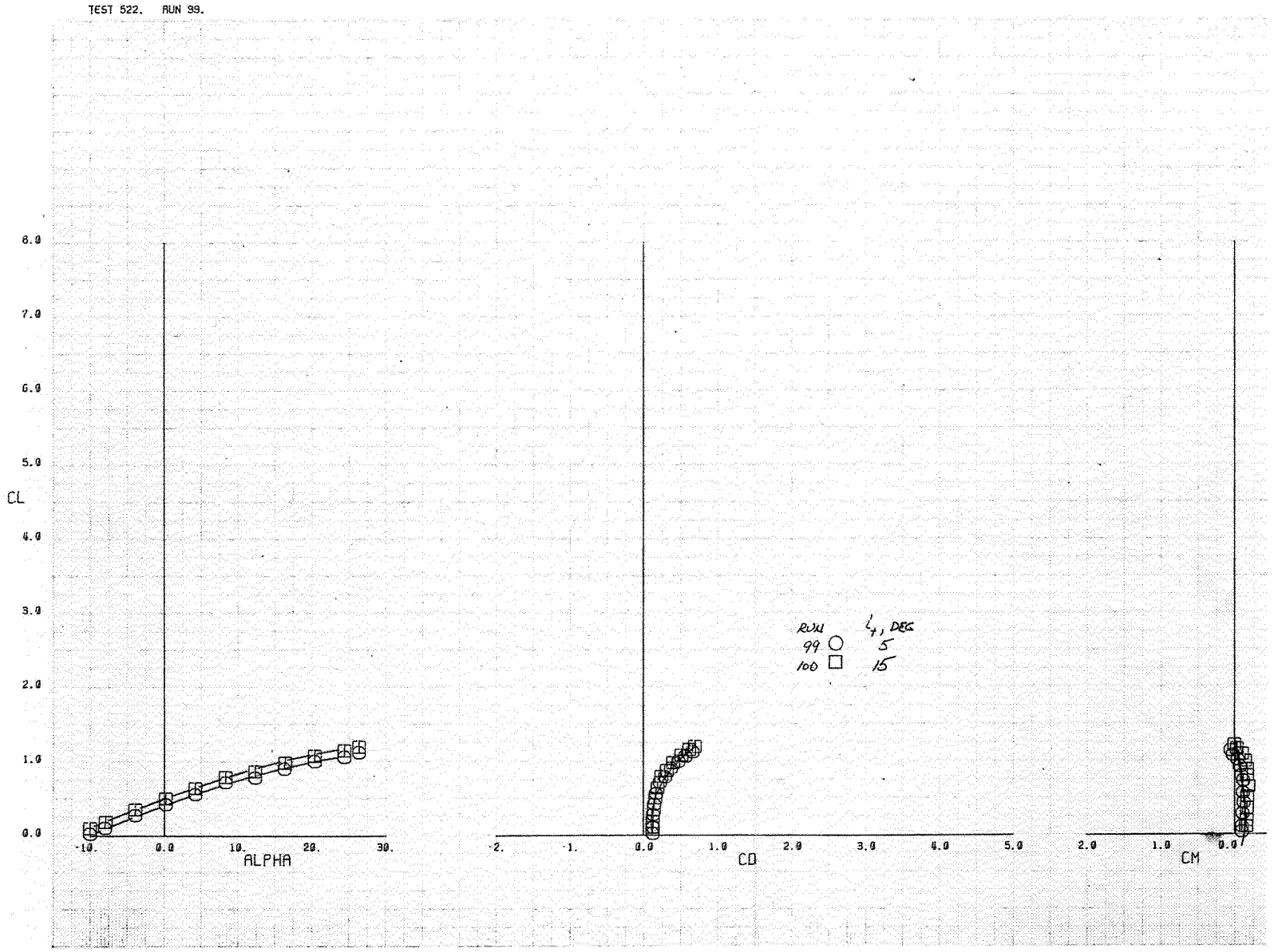

(b) Horizontal tail on, q_∞ = 699 N/m^2 (14.6 lb/ft^2).

Figure 14 - Concluded.

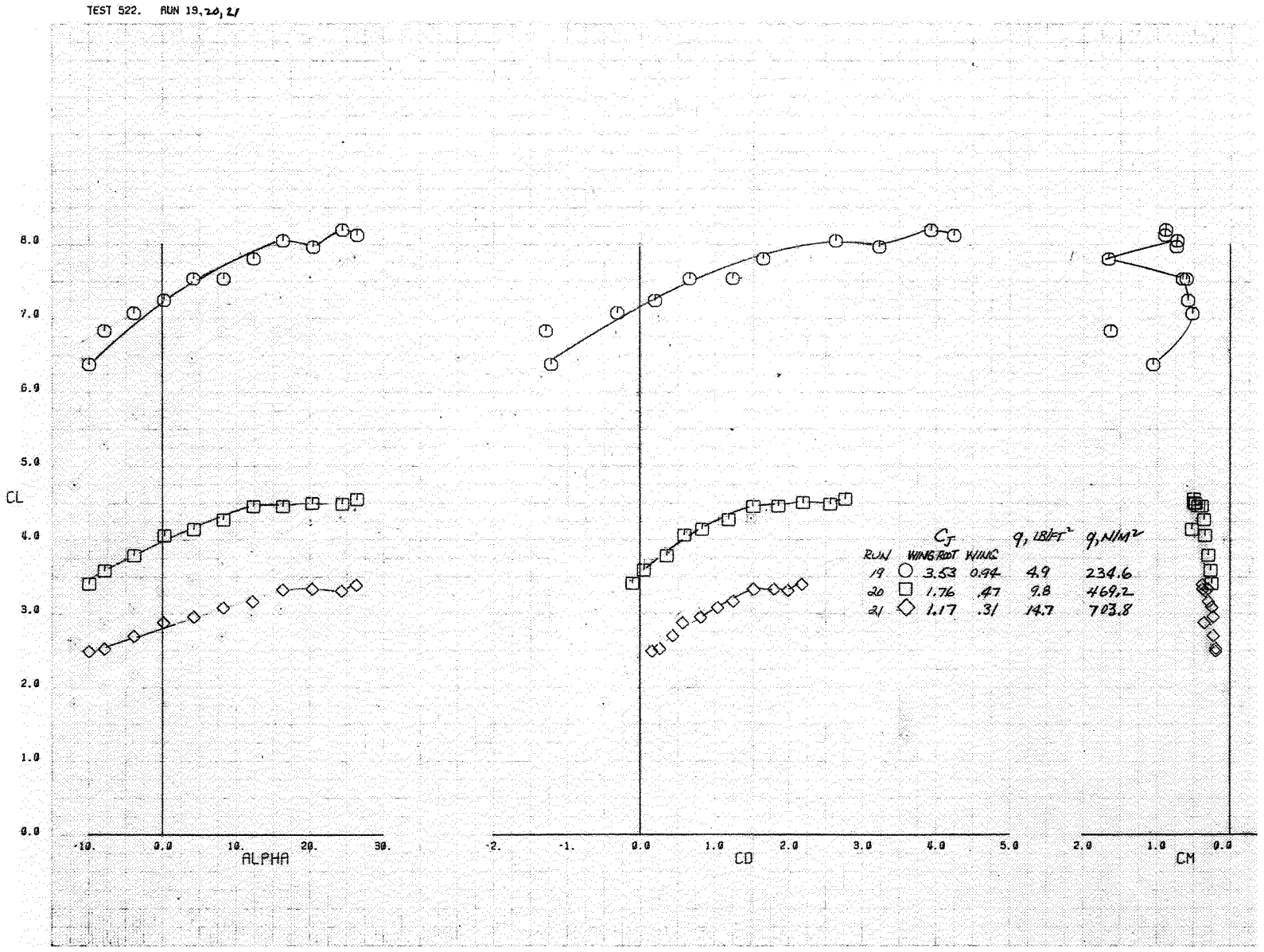

Figure 15.- Longitudinal characteristics of the model with wing root and wing augmentors operating; δ_f = 30°, RPR = 2.3, wing root DAR = 1.6, wing root augmentor exit rake off, horizontal tail off.

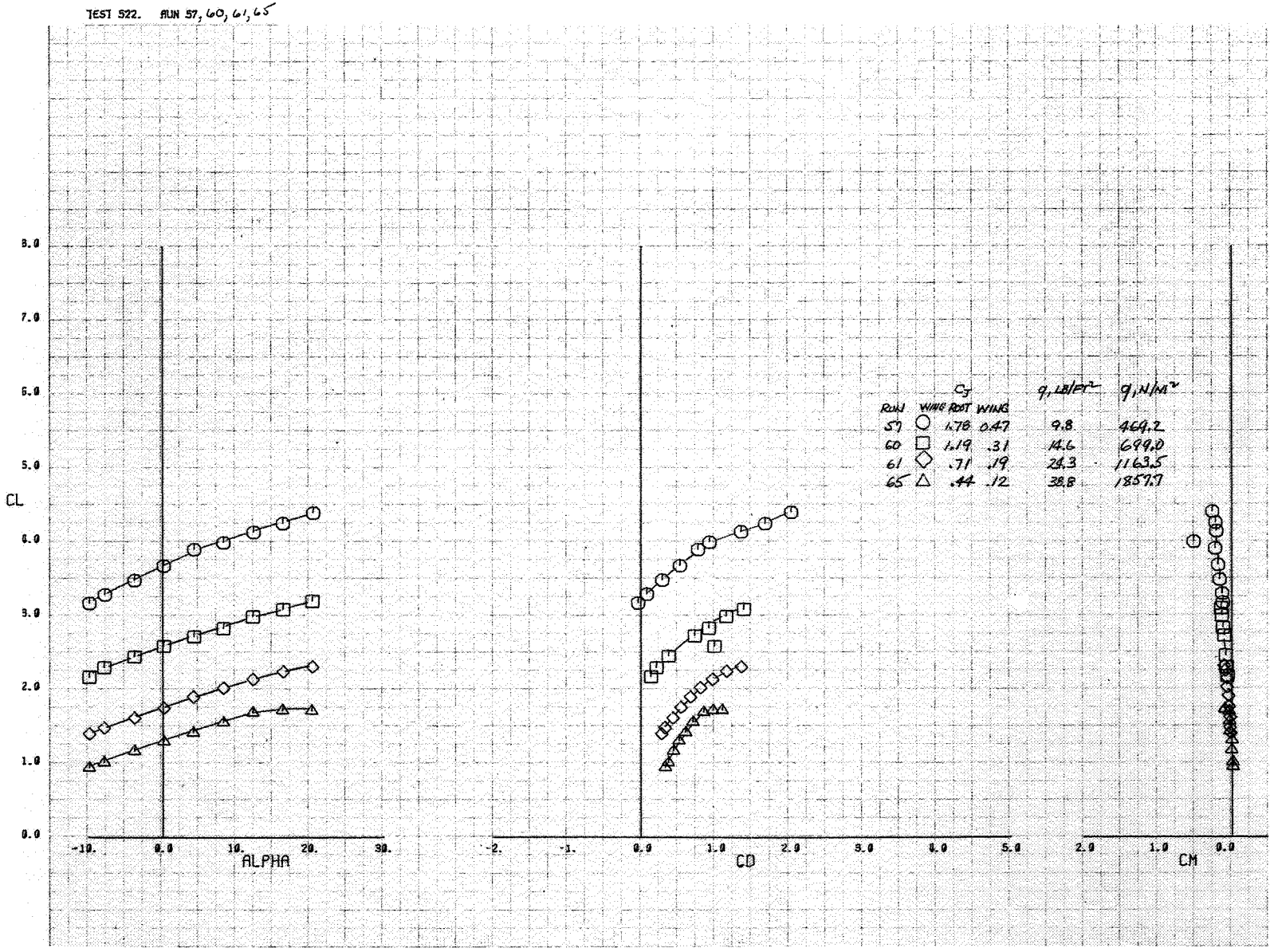

Figure 16.- Longitudinal characteristics of the model with wing root and wing augmentors operating; δ_f = 30°, RPR = 2.3, wing root DAR = 1.0, wing root augmentor exit rake off, horizontal tail off.

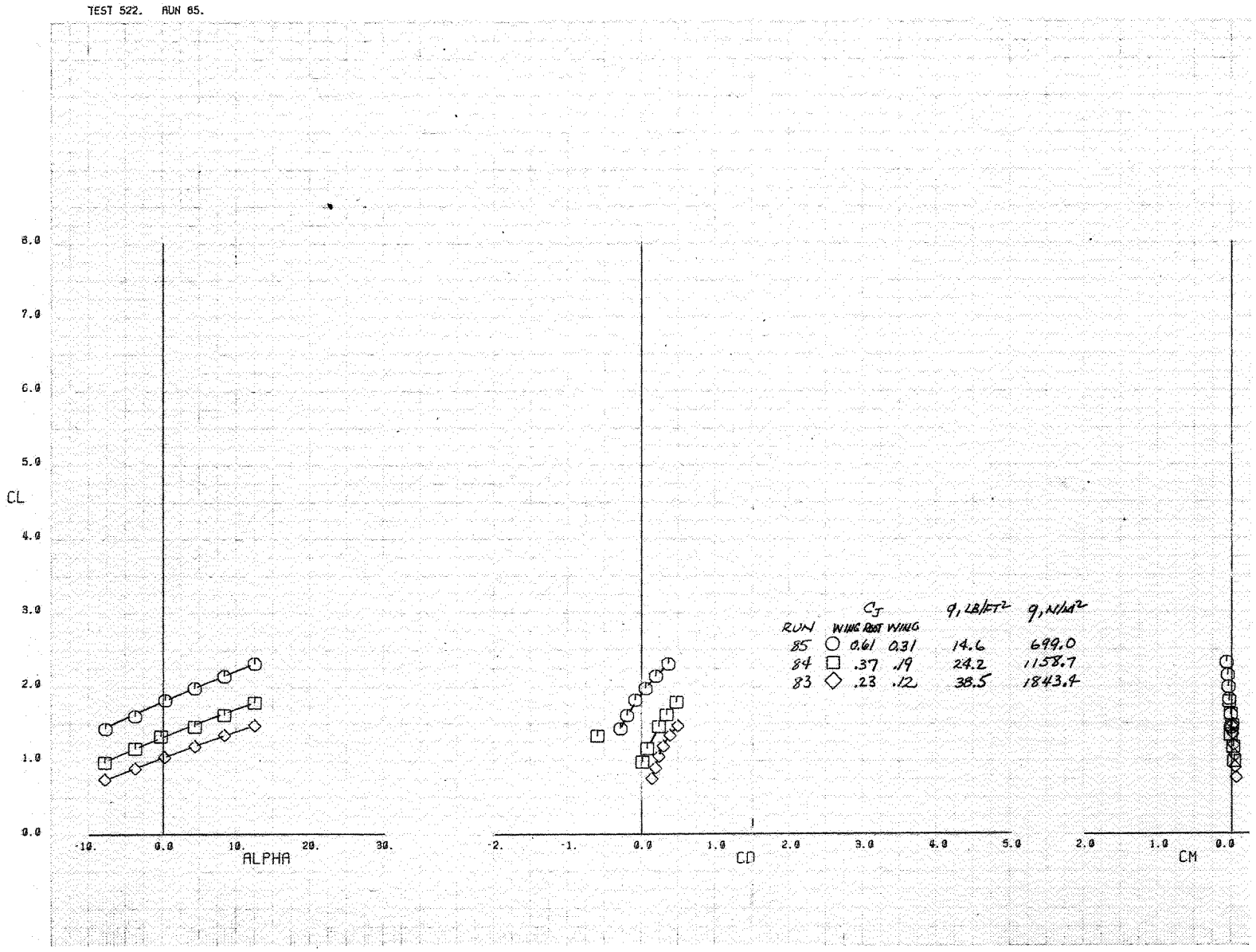

Figure 17.- Longitudinal characteristics of the model with one-half the wing root augmentor nozzle thrust; δ_f = 30°, RPR = 2.3, wing root DAR = 1.0, wing root augmentor exit rake off, horizontal tail off.

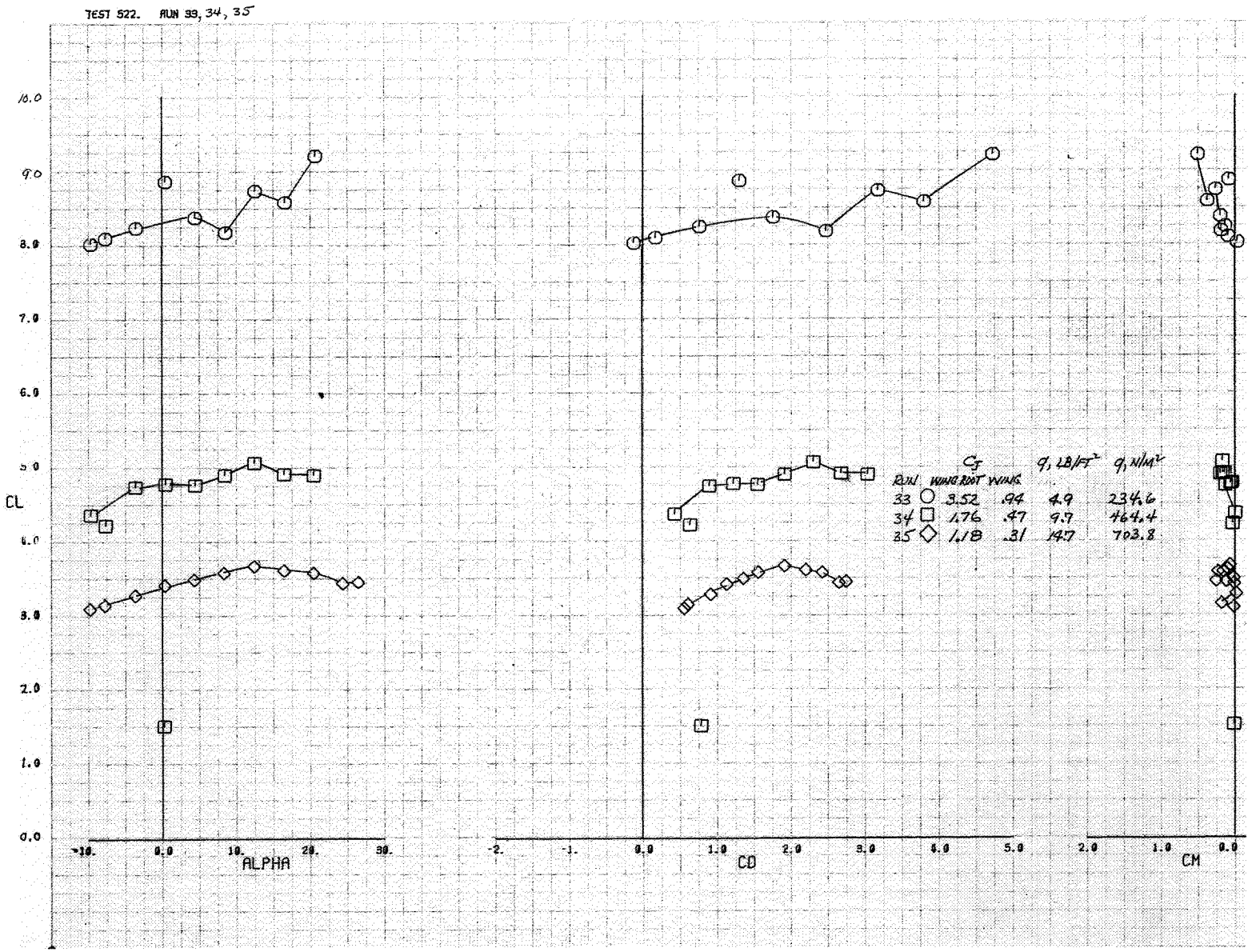

(a) Horizontal tail off.

Figure 18.- Longitudinal characteristics of the model with wing root and wing augmentors operating; δ_f = 60°, RPR = 2.3, wing root DAR = 1.6, wing root augmentor exit rake on.

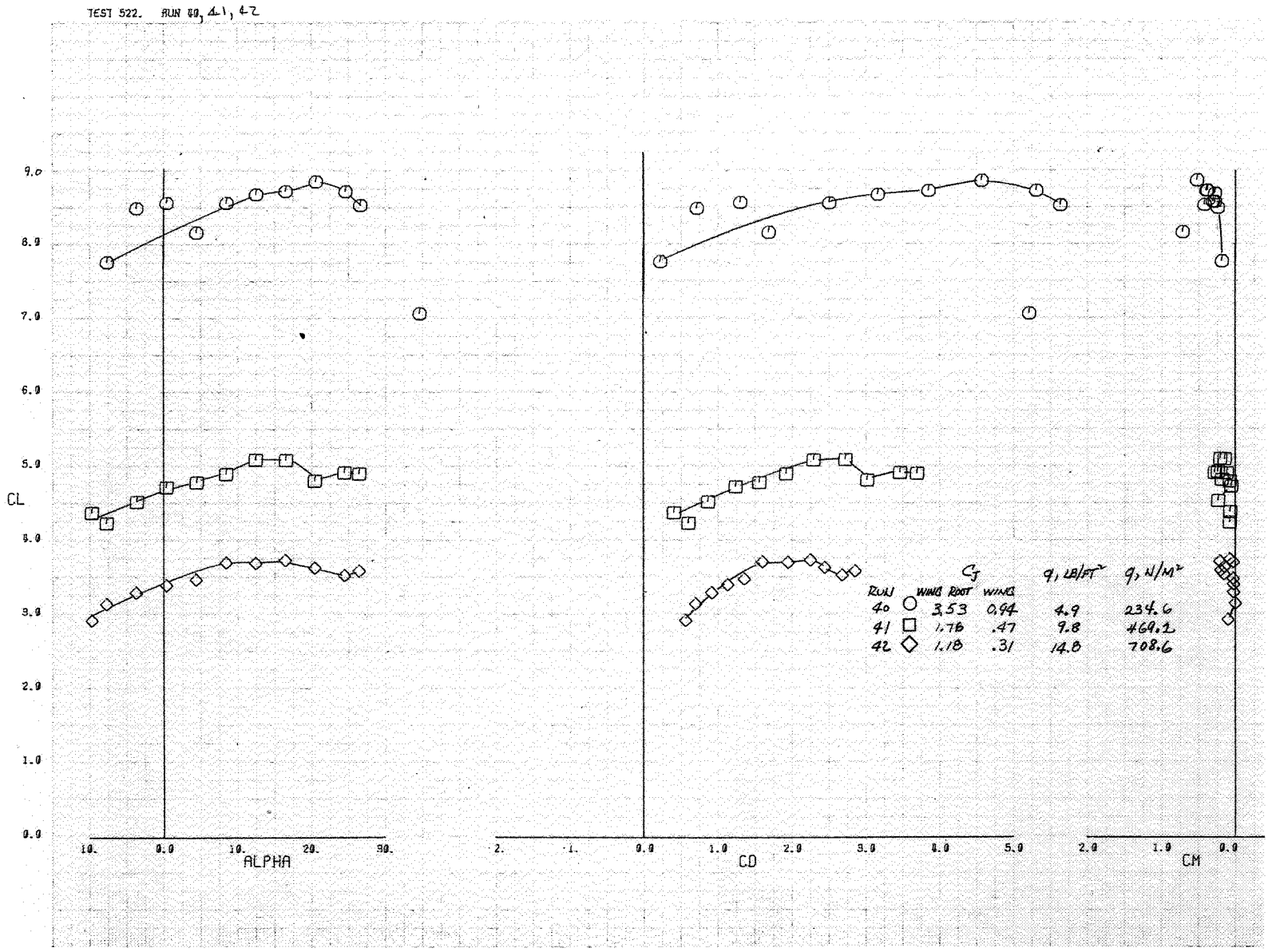

(b) $i_t = 15°$

Figure 18 – C cluded.

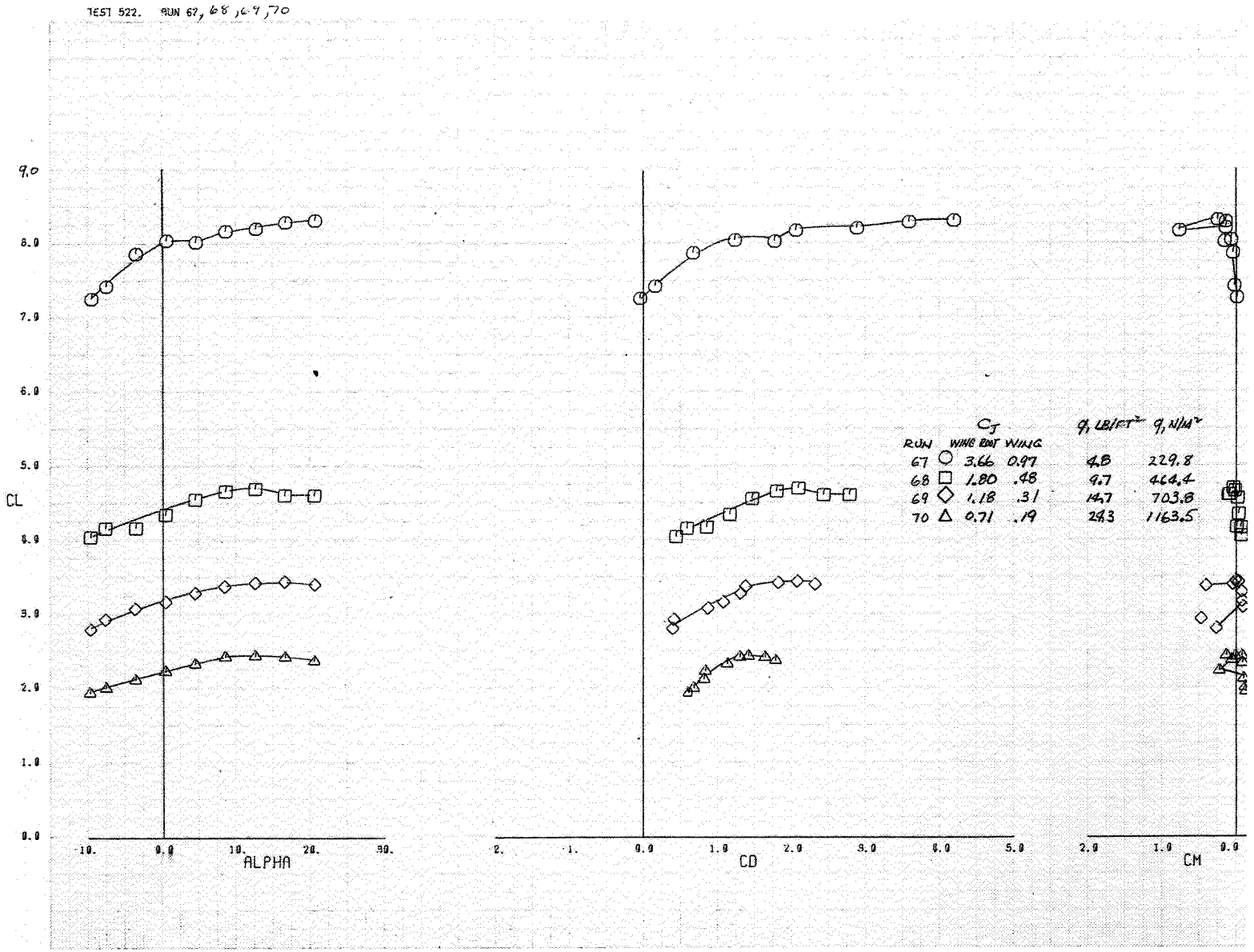

(a) Full-nozzle thrust.

Figure 19.- Longitudinal characteristics of the model with several wing root augmentor nozzle thrust values; δ_f = 60°, RPR = 2.3, wing root DAR = 1.0, wing root augmentor exit rake off, horizontal tail off.

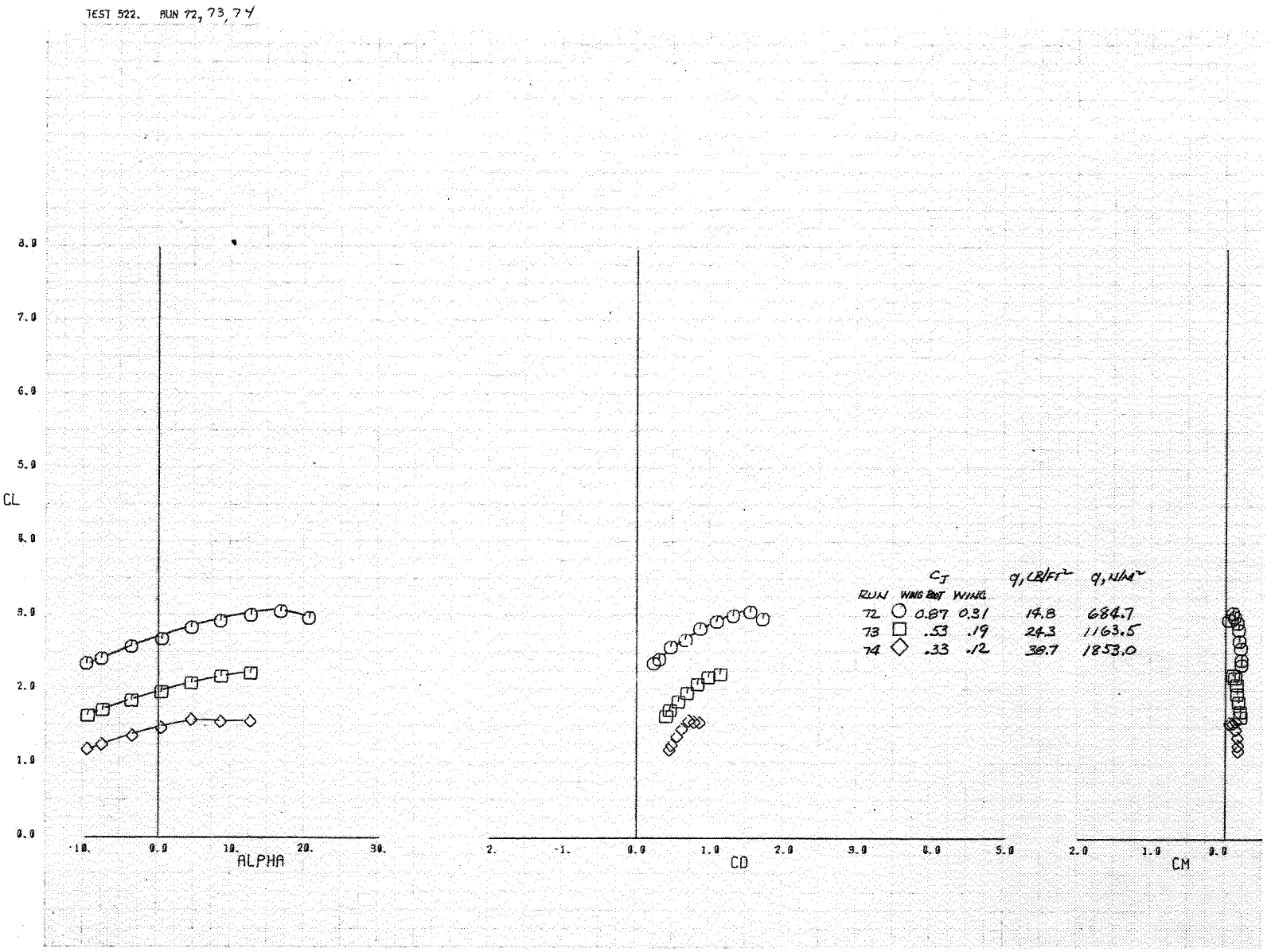

(b) 3/4-nozzle thrust.

Figure 19.- Continued.

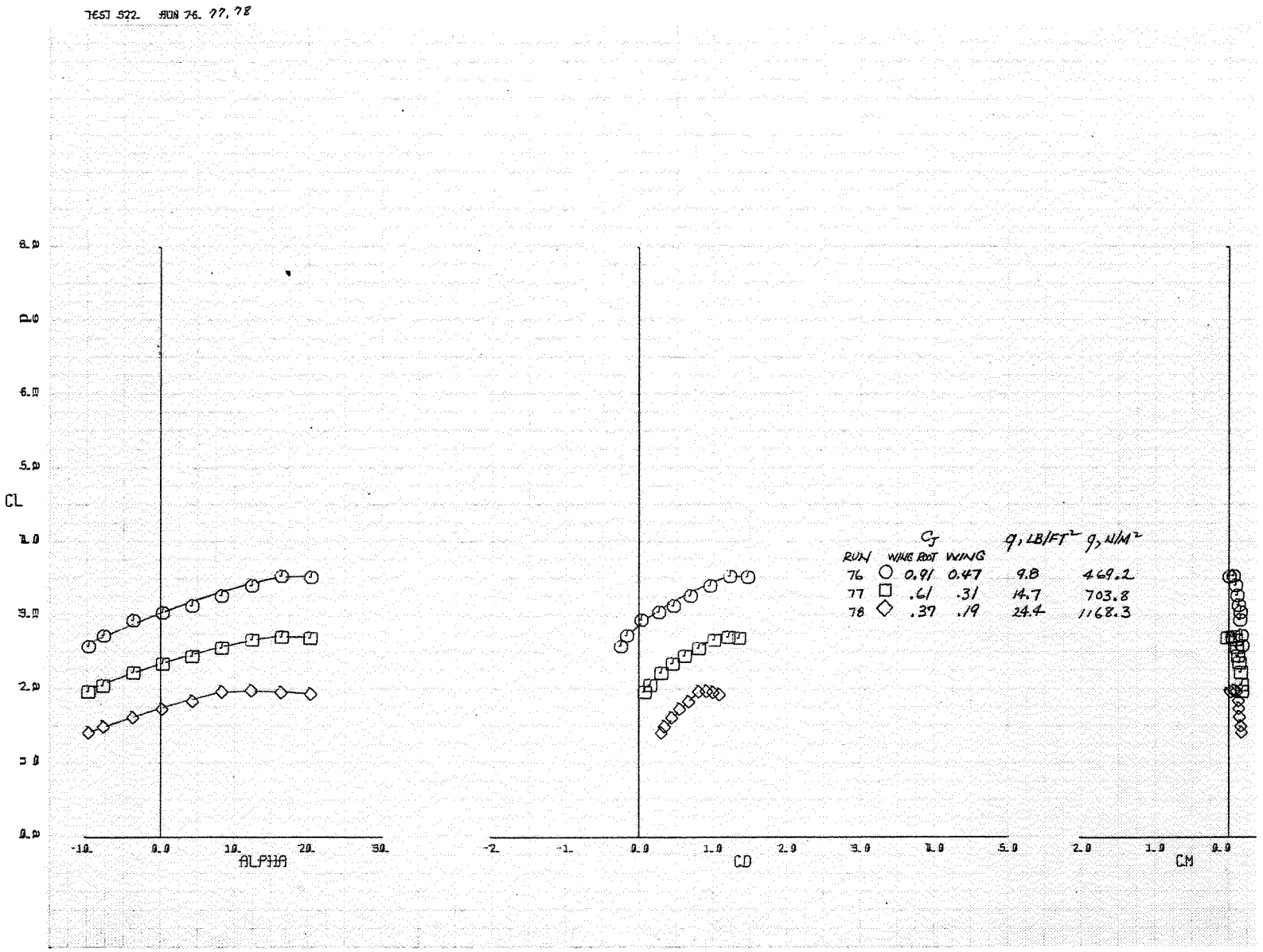

(c) 1/2-nozzle thrust.

Figure 19.- Concluded.

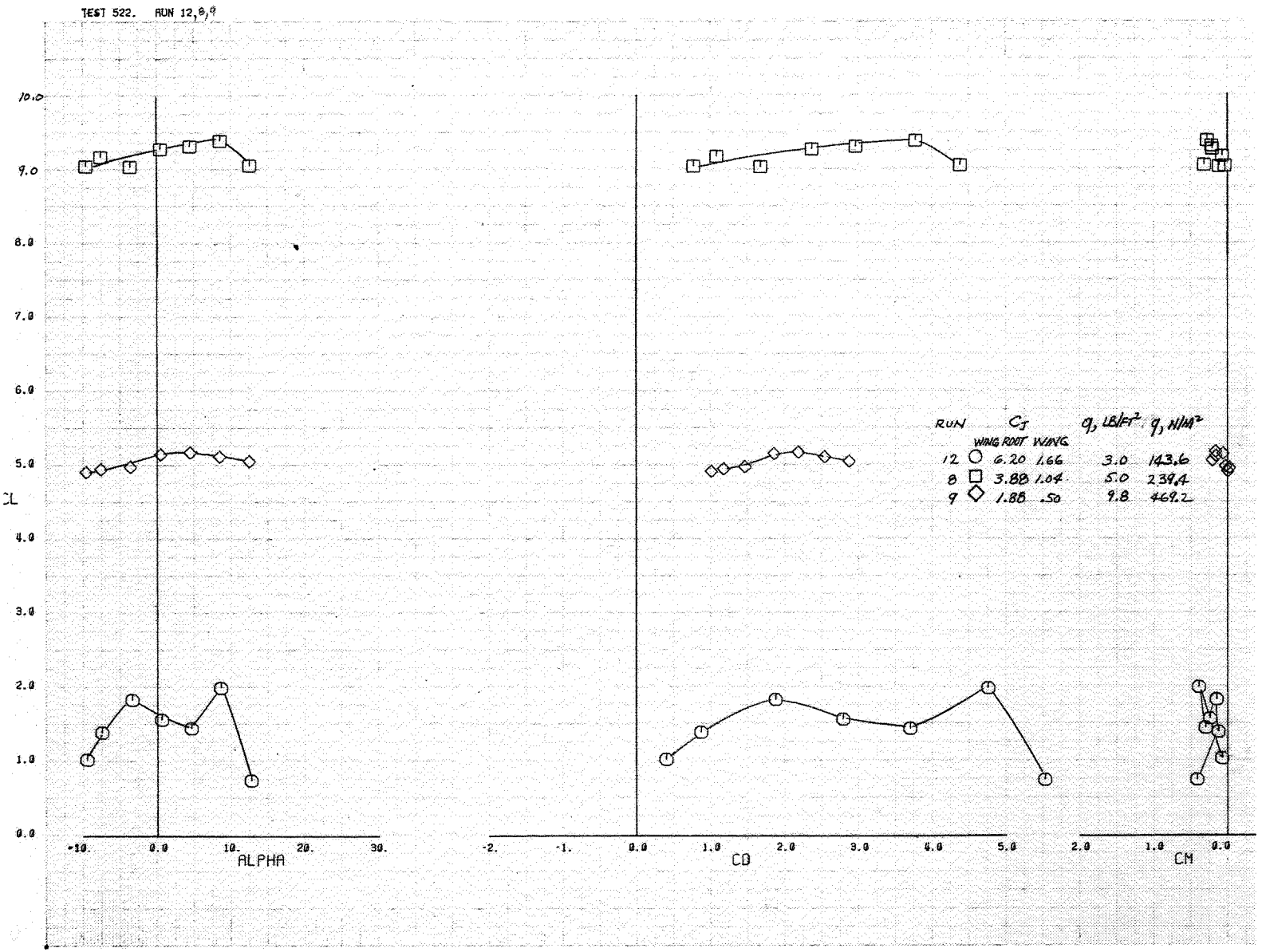

Figure 20.- Longitudinal characteristics of the model with wing root and wing augmentors operating; δ_f = 90°, RPR = 2.4, wing root DAR = 1.6, wing root augmentor exit rake off, horizontal tail off.

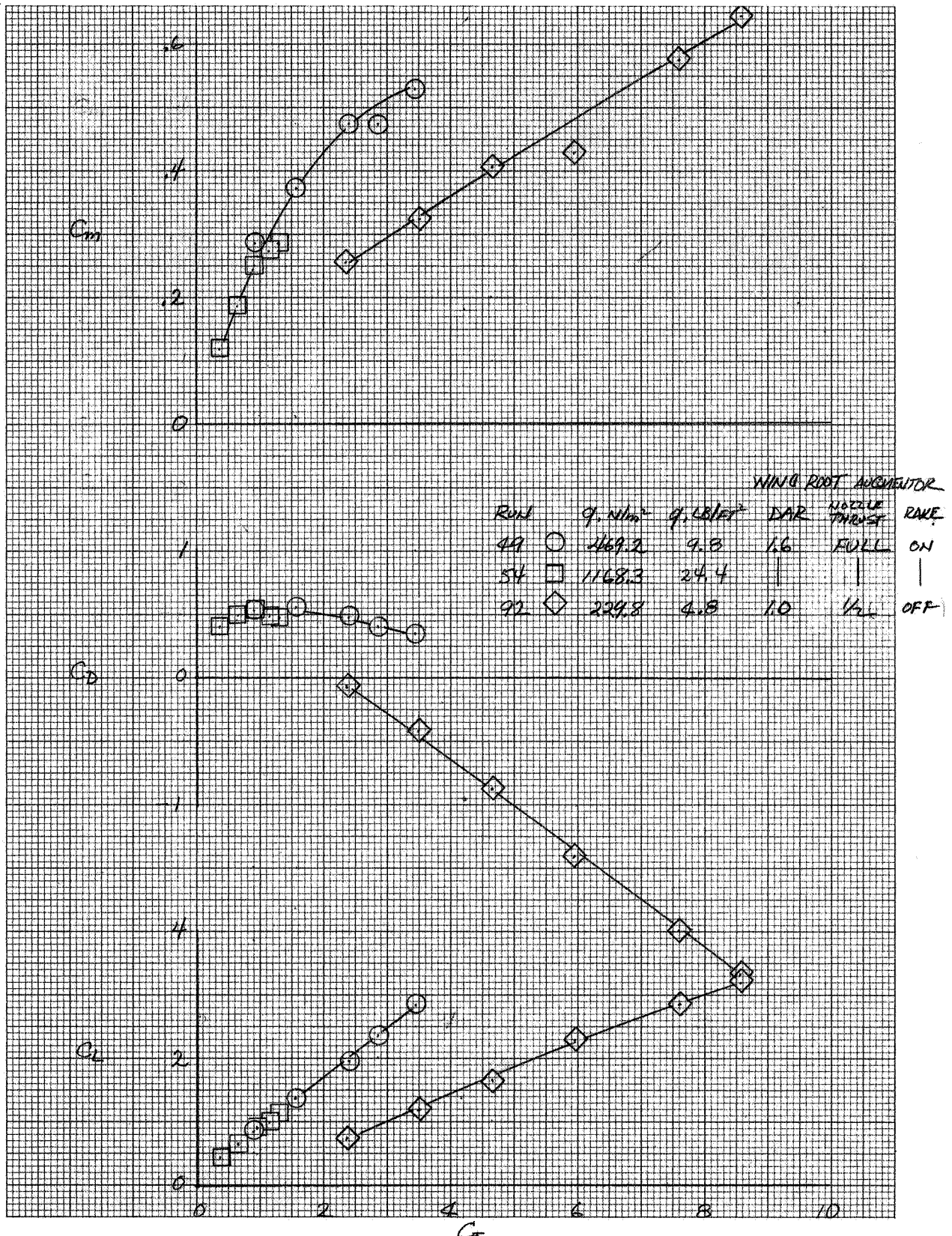

Figure 21.– Variation of C_L, C_D, C_m with $C_{J_{aug}}$; $\delta_f = 0°$, $\alpha_u = 0°$, horizontal tail off.

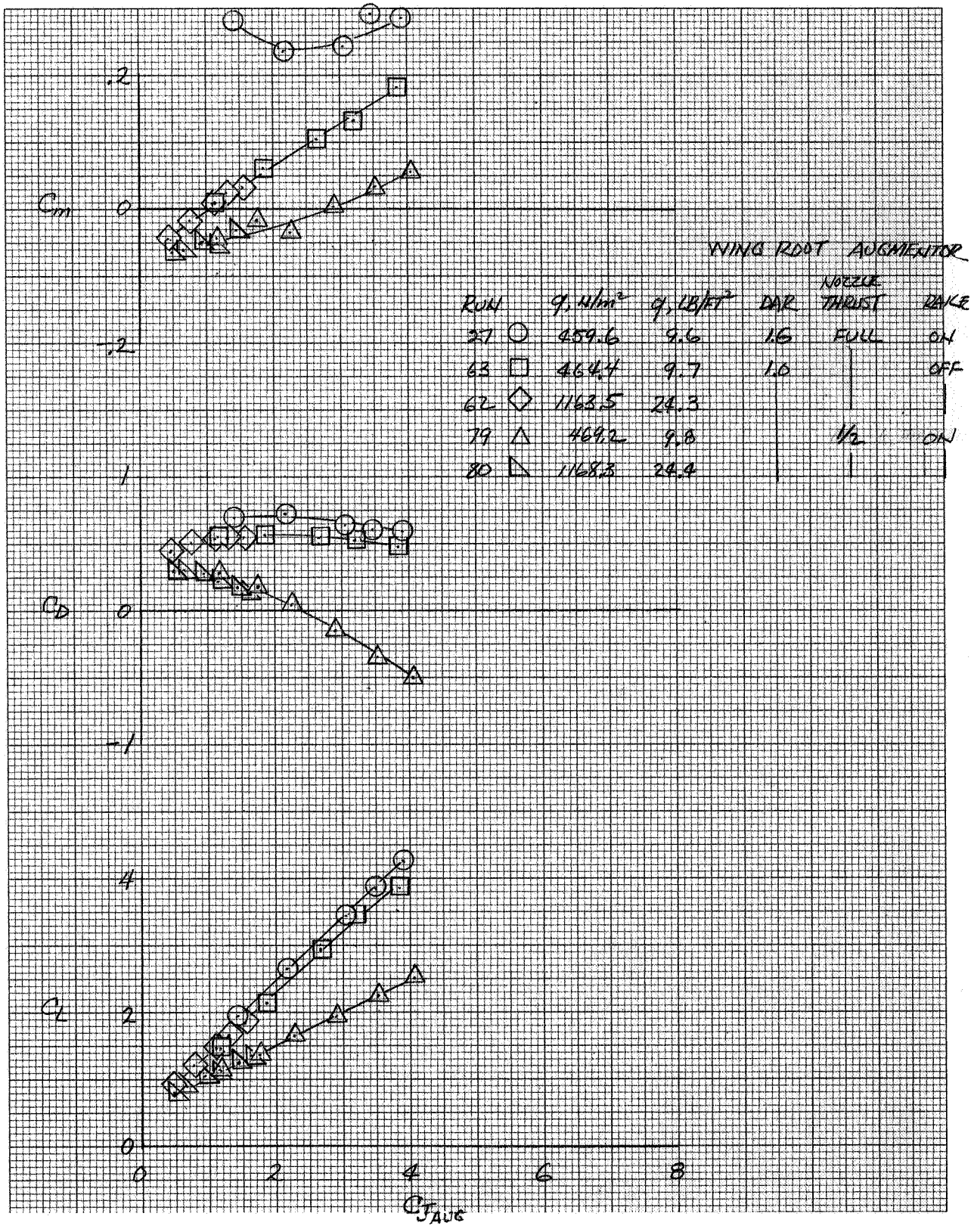

Figure 22.- Variation of C_L, C_D, C_m with $C_{J_{aug}}$; $\delta_f = 30°$, $\alpha_u = 0°$, horizontal tail off.

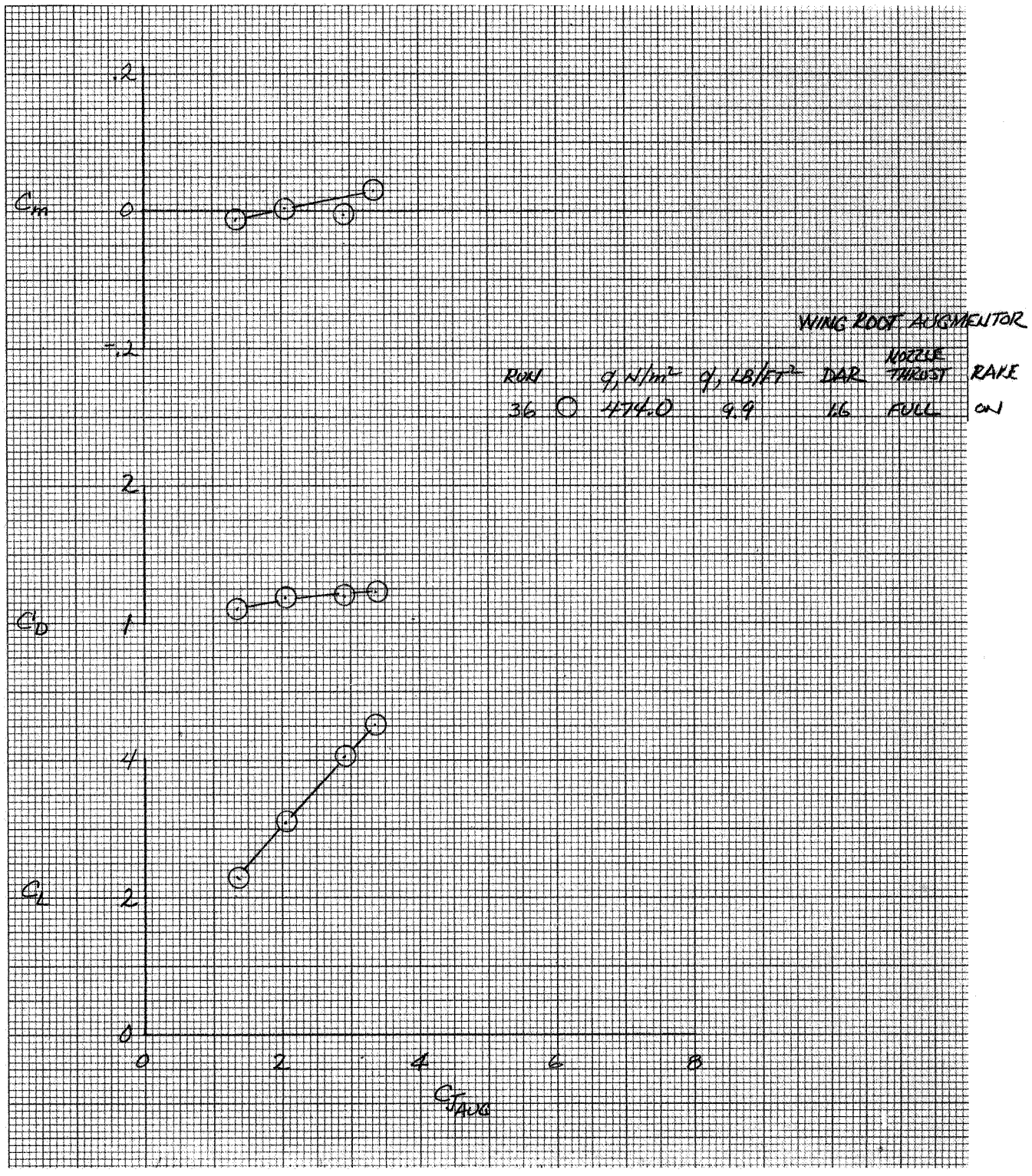

Figure 23.– Variation of C_L, C_D, C_m with $C_{J_{aug}}$; $\delta_f = 60°$, $\alpha_u = 0"$, horizontal tail off.

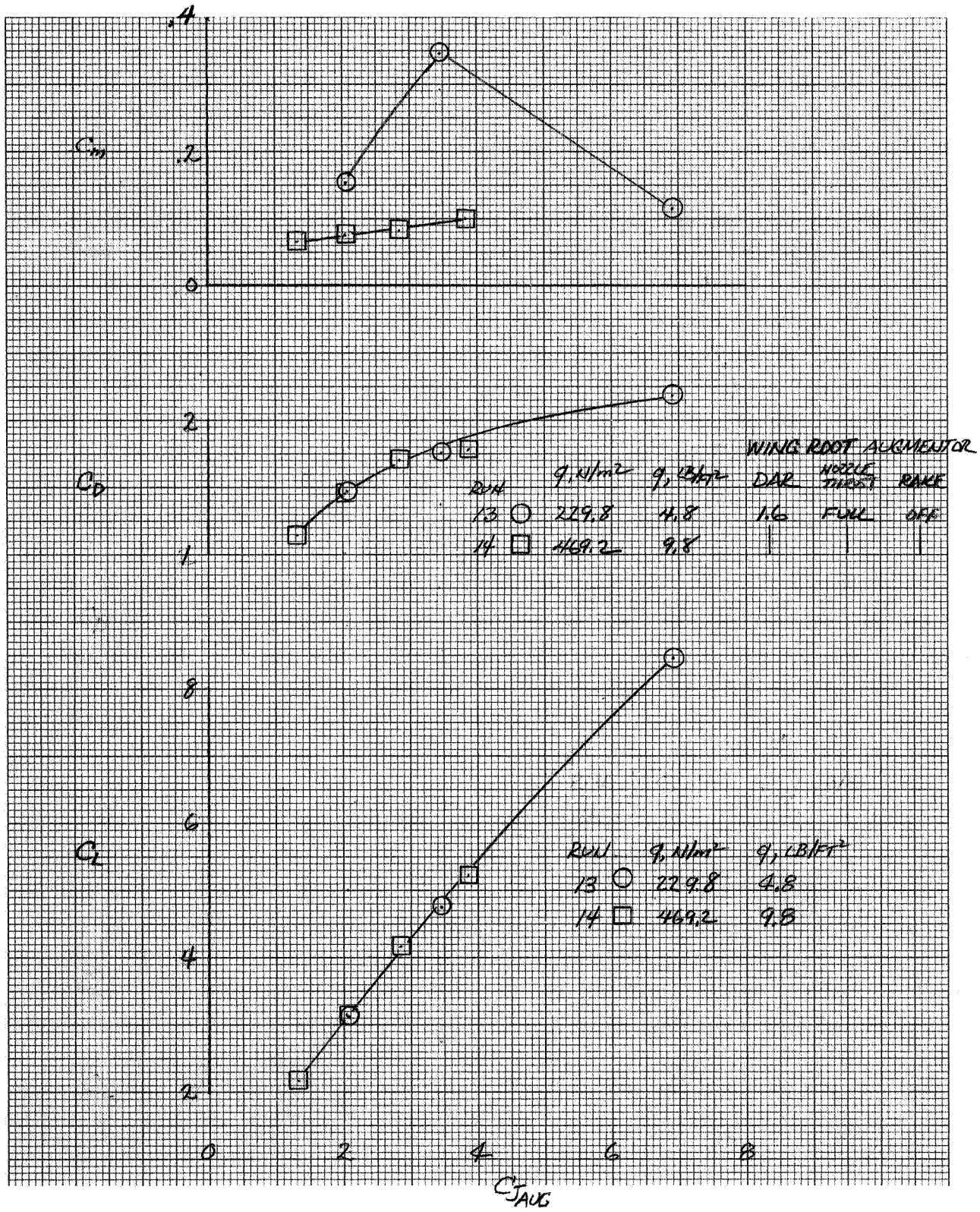

Figure 24.- Variation of C_L, C_D, C_m with $C_{J_{aug}}$; $\delta_f = 90°$, $\alpha_u = 0°$, horizontal tail off.

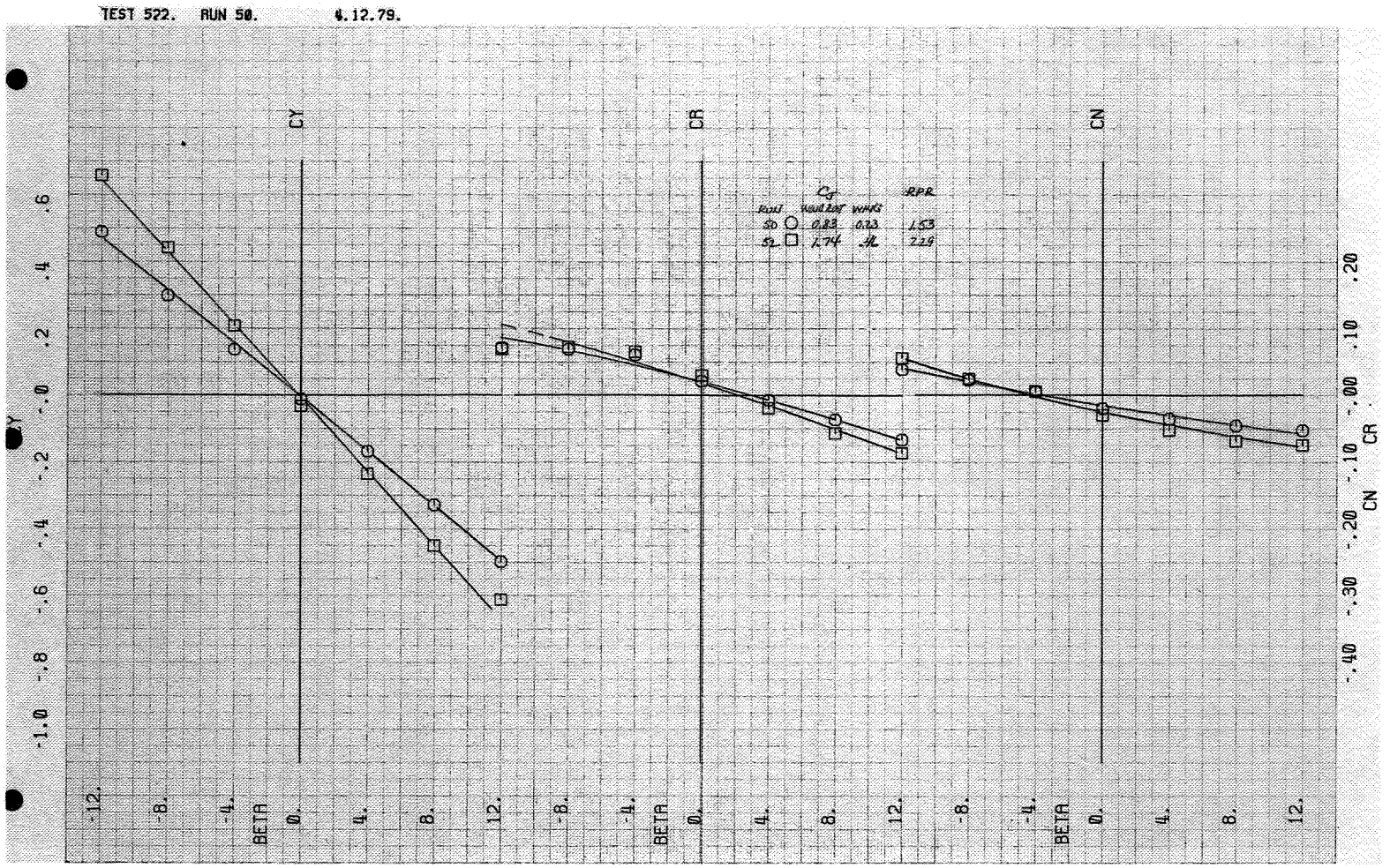

Figure 25.- Variation of C_Y, C_R, C_N with angle of sideslip; $\delta_f = 0°$, $\alpha_u = 0°$, wing root DAR = 1.6, wing root augmentor exit rake on, horizontal tail off

Figure 26.- Variation of C_Y, C_R, C_N with sideslip; wing spoiler augmentor inlet and diverter fuser door closed, $\delta_{arm} = 0°$, power off $q = 9.0$ N/m^2 (14.6 lb/ft^2), horizontal tail off.

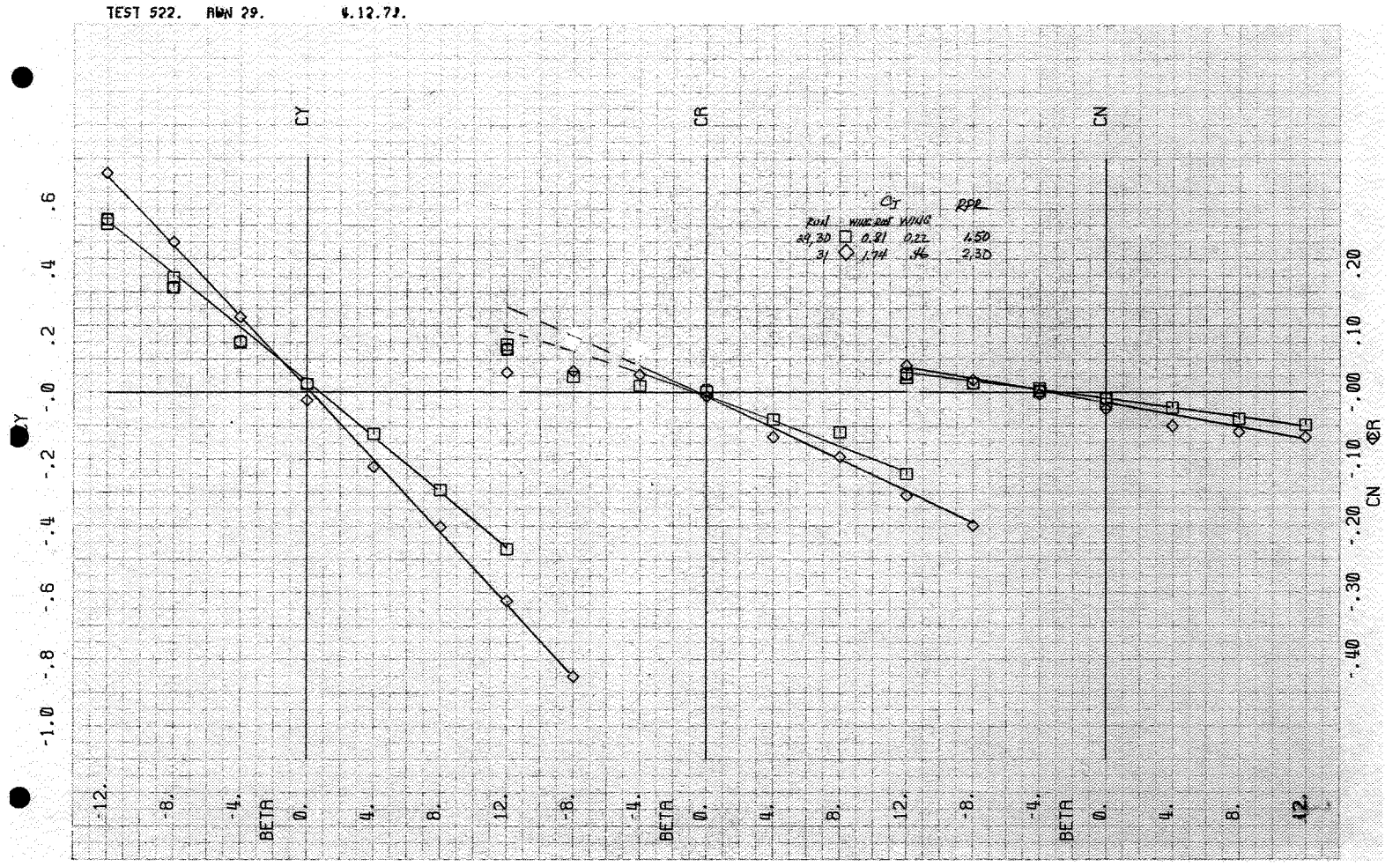

Figure 27.- Variation of C_Y, C_R, C_N with angle of sideslip; $\delta_f = 30°$, $\alpha_u = 0°$, wing root DAR = 1.6, wing root augmentor exit rake on, horizontal tail off.

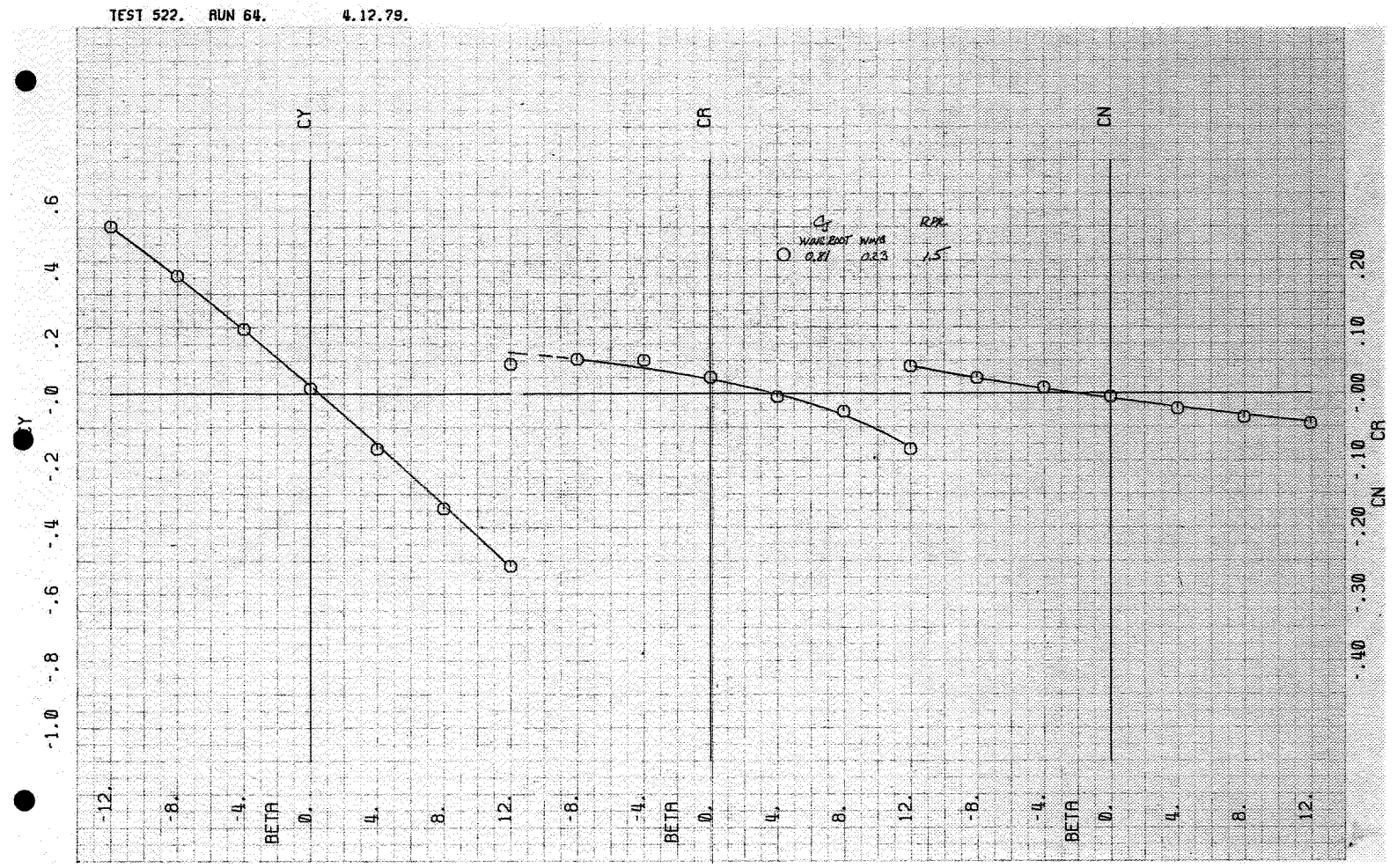

Figure 28.- Variation of C_Y, C_R, C_N with angle of sideslip; $\delta_f = 30°$, $\alpha_u = 0°$, wing root DAR = 1.0, wing root augmentor rake off, $q_\infty = 464$ ⊏ N/m^2 (9.8 lb/ft^2), horizontal tail off.

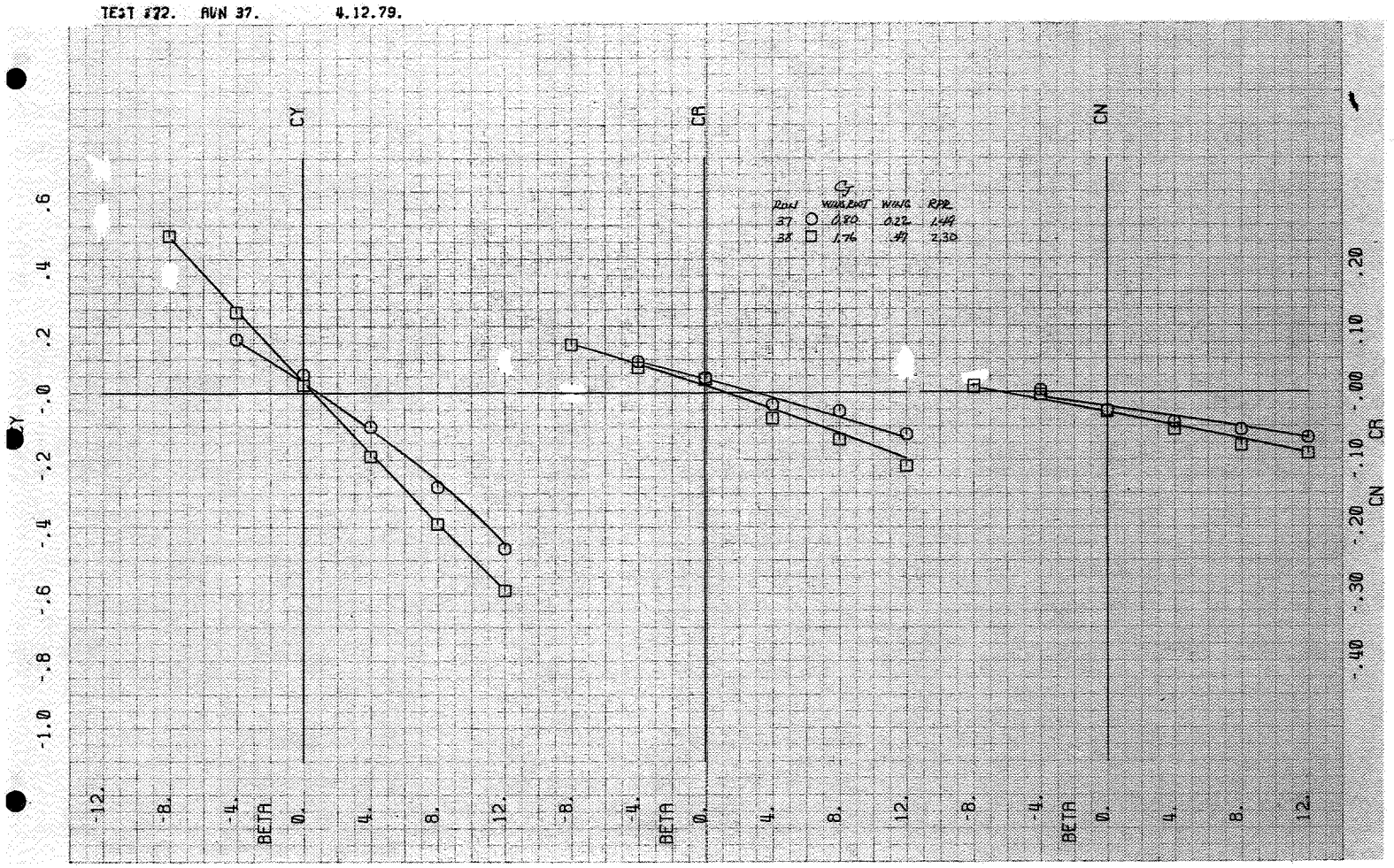

Figure 29.- Variation of C_Y, C_R, C_N with angle of sideslip; $\delta_f = 60°$, $\alpha_u = 0°$, wing root DAR = 1.6, wing root augmentor exit rake on, $q_\infty = 464.4$ N/m^2 (9.7 lb/ft^2), horizontal tail off.

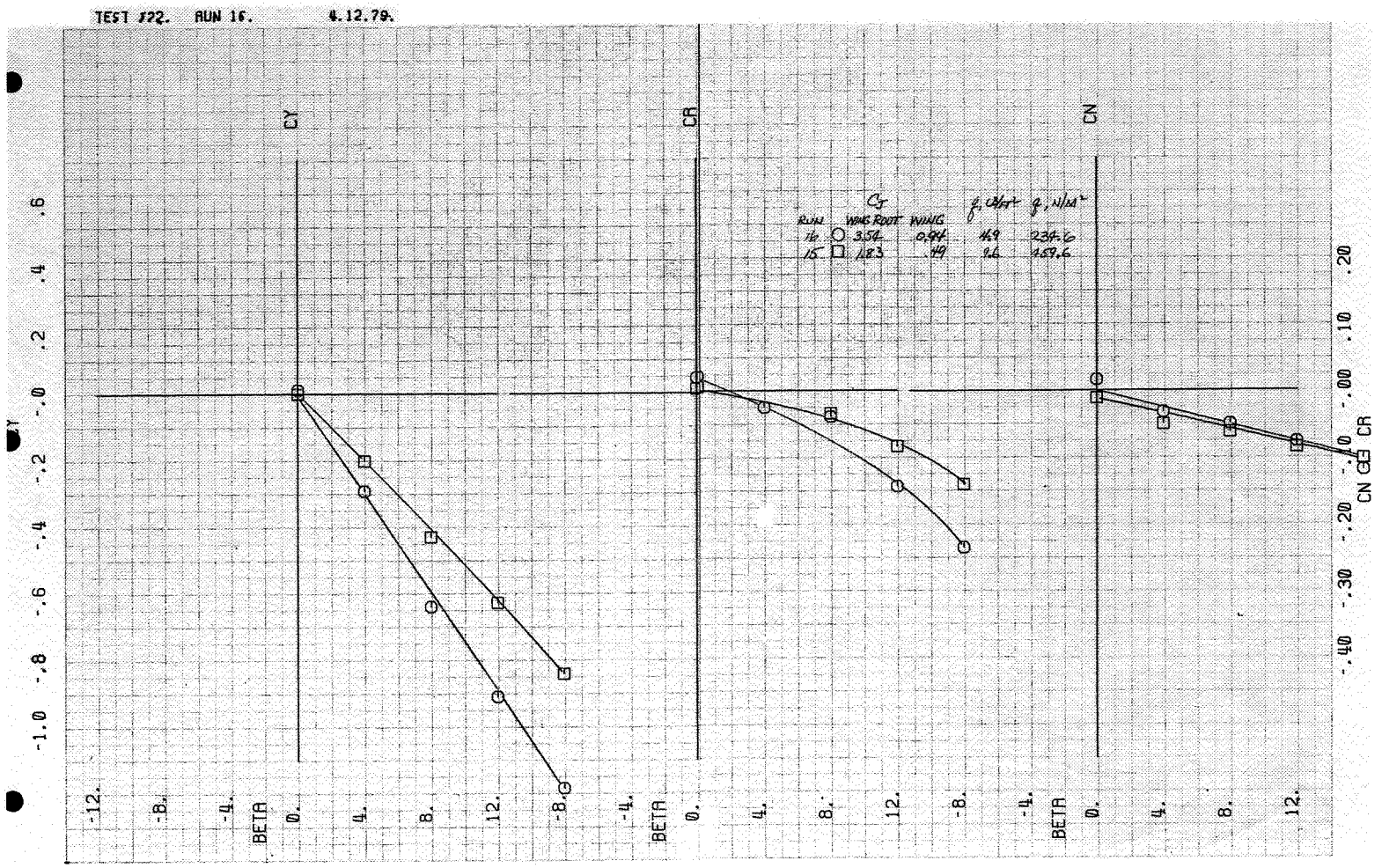

Figure 30.- Variation of C_Y, C_R, C_N with angle of sideslip; $\delta_f = 90°$, $\alpha_u = 0°$, wing root DAR = 1.6, wing augmentor exit rake off, horizontal tail off.

1. Report No.	2. Government Accession No.	3. Recipient's Catalog No.
NASA TM-78589		

4. Title and Subtitle	5. Report Date
WIND TUNNEL INVESTIGATION OF A LARGE-SCALE VTOL AIRCRAFT MODEL WITH WING ROOT AND WING THRUST AUGMENTORS	6. Performing Organization Code

7. Author(s)	8. Performing Organization Report No.
Kiyoshi Aoyagi and Thomas N. Aiken	A-7823
	10. Work Unit No. 518-58-21
9. Performing Organization Name and Address	11. Contract or Grant No.
Ames Research Center, NASA Moffett Field, Calif. 94035	
	13. Type of Report and Period Covered
12. Sponsoring Agency Name and Address	Technical Memorandum
National Aeronautics and Space Administration Washington, D.C. 20546	14. Sponsoring Agency Code

16. Abstract

Tests were conducted in the Ames 40- by 80-Foot Wind Tunnel to determine the aerodynamic characteristics of a large-scale V/STOL aircraft model with thrust augmentors. The model had a double-delta wing of aspect ratio (AR) 1.65 with augmentors located in the wing root and the wing trailing edge. The supply air for the augmentor primary nozzles was provided by the YJ-97 turbojet engine. The airflow was apportioned approximately 74% to the wing root augmentor and 24% to wing augmentor. Results were obtained at several trailing-edge flap deflections with the nozzle jet-momentum coefficients ranging from 0 to 7.9.

Three-component longitudinal data are presented with the augmentor operating with and without the horizontal tail. A limited amount of six-component data are also presented.

17. Key Words (Suggested by Author(s))	18. Distribution Statement
V/STOL Ejector Aerodynamics	Unlimited STAR Category - 02

19. Security Classif. (of this report)	20. Security Classif. (of this page)	21. No. of Pages	22. Price*
Unclassified	Unclassified	60	$5.25